RESEARCH   **Open Access**

A novel transparent cabin used in the classroom during the coronavirus pandemic: a CFD analysis

Mennatullah ElShimi[1]*, Samy M. Morcos[1], Galal M. Mostafa[1], Essam E. Khalil[1], Gamal A. El-Hariry[1] and Ahmed ElDegwy[1]

*Correspondence:
menna_mohammed_
ahmed_1993@yahoo.com

[1] Mechanical Power Engineering Department, Faculty of Engineering, Cairo University, Giza 12613, Egypt

Abstract

A coronavirus family is a diverse group of many viruses. Coronavirus disease 19 (COVID-19) spreads when an infected person breathes out droplets and very small particles that contain the virus. These droplets and particles can be breathed in by other people or land on their eyes, noses, or mouths. In this paper, the airflow distribution and the movement of coronavirus particles during normal breathing and sneezing in classrooms have been studied using a CFD model developed in ANSYS® 2022R2. The objective is to find ways to control the spread of the virus that enable us to practice academic activity and deal normally with the pandemic and the spread of the disease. Experiments were done with more than one turbulence model to know which was closest to the experiments as well as to determine the best number of meshes in the classroom. The effect of turbulent dispersion on particles is resolved using a discrete random walk model for the discrete phase and the RANS model for the continuous phase in a coupled Eulerian–Lagrangian method. Furthermore, that is done in two scenarios: the first is to find the best ventilation configuration by investigating the following parameters: the effect of air change per hour, the height of the air inlets and outlets, and the infected student's position. The second is to control the spread of the coronavirus in the classroom in the event of sneezing from an infected student by placing cabins and an air filter with optimal design installed at the top around each student. It was found that optimal ventilation is achieved when fresh air enters from the side walls of the classroom at a distance of 1 m from the floor and the air exits from the ceiling in the form of two rows, and the rate change of air per hour (ACH) is 4, which leads to energy savings. In addition, a novel transparent cabin is designed for the student to sit in while in the classroom, consisting of a high-efficiency particulate air filter (HEPA) that collects any contamination and recirculates it from the top of the cabin back into the classroom with different fan speeds. Through this study, this cabin with a filter was successfully able to prevent any sneeze particles inside from reaching the rest of the students in the classroom.

Highlights

1. More than 12 different air conditioning systems were examined in the classroom for thermal comfort and energy efficiency, with the best one being selected first.

2. In the classroom, saliva droplets are studied using CFD simulations using the Euler–Lagrange technique.

3. Experiments were done with more than one turbulence model to know which was closest to the experiments, as well as to determine the best number of meshes in the classroom.

4. The reduction of infection in the case of breathing or sneezing has been studied.

5. A novel cabin with a HEPA filter was developed, and its impact on decreasing infection was investigated.

Keywords: CFD, Infection control, Educational buildings, IAQ, COVID-19

Introduction

The coronavirus pandemic that has engulfed the globe for the first five months of 2020 has transformed the pace, manner, and character of our lives. The coronavirus family is a large category that includes several viruses. Some of these can cause the common cold. The coronaviruses that cause MERS, or Middle Eastern respiratory syndrome, and SARS got their start in this way. In 2019, a brand-new coronavirus was connected to an epidemic of illness that started in China. In March 2020, the World Health Organization (WHO) declared the COVID-19 outbreak a pandemic. The economics, psychology, and educational systems were just a few of the sectors that the coronavirus pandemic had a significant influence on. COVID-19 spreads when an infected individual exhales droplets and very small particles harboring the virus. These droplets and particles might be inhaled by other people, or they could contact their lips, noses, or eyes. They may occasionally infect the surfaces they come into contact with [1]. The COVID-19 pandemic has led to the conduct of many studies to analyze the risks resulting from the spread of the virus and to work to limit the spread of the virus in many applications. Kong et al. [2] analyzed four categories of air distribution patterns, including top supply and exhaust, side supply and exhaust, and bottom supply and exhaust. They considered two experimental scenarios to calculate the movement of particles produced by patients. The study found that the optimal ventilation layout had the top diffusers on the sidewall serving as a supply and the lower diffusers acting as a return. The study also used computational fluid dynamics (CFD) simulations to characterize the dispersion of contaminated droplets in the ward. Kumar et al. [3] modeled various HVAC settings. According to a study, in order to prevent the transmission of airborne infections, high ventilation rate requirements might be altered in both new and existing hospital designs. Chillon et al. [4] used computational fluid dynamics (CFD) modeling to simulate a high-risk scenario, such as a lift in a hospital. A rack for air renewal and an extraction fan were provided for the barrier. A cough, a sneeze, and a continuous speech were all studied. The fan was assessed as having a strong performance in distributing particles while also being able to expel 60% of tiny droplets. Dbouk et al. [5] examined three flow scenarios, including inlet and outlet placement in lifts and air purifier operations. The location of inlets and outputs significantly impacts flow circulation and droplet dispersion. Air filters do not totally prevent airborne transmission, although employing input and exit pairs reduces droplet

ElShimi *et al. Journal of Engineering and Applied Science*   (2024) 71:19

Page 3 of 39

dispersal. The placement and design of ventilation systems and air purifiers significantly impact droplet dispersion and airborne virus transmission. Therefore, flow dynamics in limited space must be considered in engineering designs for such systems. Yamakawa et al. [6] examined the prolonged dispersion of fresh coronavirus-laden droplets in the classroom's air as a result of the instructor's coughing. According to the study's findings, there was a significant danger of sustained airborne transmission of virus-containing droplets when the classroom ventilation outlet flow was low (between 4.3 and 8.6 cm/s). The findings showed that pupils can prevent contact with the virus-carrying droplets by maintaining a significant distance from the instructor (5.5 m), which is more than twice as far as the generally advised social distancing guidelines. Ascione et al. [7] examined the air diffusion capabilities of four layouts. To make indoor university classrooms safe and sustainable, they provided useful advice and directions for remodeling educational structures. The results showed that while all air terminal designs offer adequate thermal comfort, the configuration with linear slot diffusers offers better results in terms of the regularity of the air distribution and its purity, as well as the creation of the most comfortable surroundings. Arpino et al. [8] investigate the dispersion of airborne droplets released in line with the instructor's position inside a lecture room over time as a function of variable ACH from the HVAC system using 3D CFD numerical simulations based on an Eulerian–Lagrangian approach. The findings show that raising the air supply rate is not always effective at reducing aerosol concentration to match the postures used by the students taking part in the class.

Adwibowo et al. [9] conducted a computational fluid dynamic study to determine the interactions between seat layout, social distance, airflow, and droplet dispersion in the indoor public area. The results suggest that increasing the distance between chairs and providing more room in public areas may reduce the danger of droplet dispersions. On the other hand, protecting while simultaneously creating a shield is far more effective at reducing dispersion and improving air quality. A facial shield is not a safe device, according to Akagi et al's [10] simulation of a sneeze against one. This is because the vortexes can get between the face and the shield and introduce 4.4% of the expelled droplets. To avoid viral infection, Kadir et al. [11] created a custom-made mask design. The spread of viruses was simulated using simulation programs on computers while the infected person was wearing masks, and the effectiveness of the wearing of different masks (i.e., traditional and custom-made masks) by someone infected with COVID-19 and other infectious diseases was compared. The simulations revealed that the customized mask design is more efficient than traditional masks since it poses a significantly lower risk of viral infection. Bahramian et al's [12] research and CFD modeling show that indoor temperature significantly impacts airflow dynamics, velocity fields, size distribution, and airborne transmission of sneeze droplets in confined environments. Time and distance from the source affect droplet number, concentration, and size distribution. The size, beginning velocity, and ambient temperature also affect the distance droplets can spread. Increased indoor temperature marginally reduces mean droplet velocity but significantly influences the number of medium and large droplets in dilute-dispersed droplets. Ying et al. [13] formulate an agent-based model of customer movement in a supermarket with a simple virus transmission model based on the amount of time a customer spends close to infectious customers. They have implemented a variety of policies, but the best one is to limit the number of customers or the

arrival rate of customers while also requiring that everyone wear a face mask. By doing this, the number of infections and the likelihood of contracting an infection in a supermarket can be greatly reduced. Li et al. [14] evaluated the possibility of airborne transmission in a restaurant in Guangzhou, China, affecting three families. They predicted the dispersion of droplets and airflow patterns using tracer gas measurements and CFD simulations. The results suggest that long-range airborne transmission of SARS-CoV-2 may occur in crowded and poorly ventilated spaces rather than in any indoor space. Srivastava et al. [15] conducted computational fluid dynamics numerical simulations to study the impact of using an ultraviolet-C (UV-C) air disinfection device (RM3 UV-C units) on COVID-19 infection risk in office buildings. The study found that the optimal method for cleaning air carrying SARS-CoV-2 is a combination of 100% outdoor air and UV-C in HVAC ducts. This reduces the risk of contamination and saves energy, making it a viable solution for reducing COVID-19 infection risk in office buildings. Ren et al. [16] used a CFD program (ANSYS Fluent) to compare several ventilation strategies in the office, including mixing ventilation (MV), zone ventilation (ZV), stratum ventilation (SV), and displacement ventilation (DV), by analyzing ventilation performance and infection risk for the optimal one. Li et al. [17] studied the impact of parallel jet spacing (PJS) on multi-jet stratum ventilation effectiveness in an office. They used the computational fluid dynamics model to evaluate thermal comfort and energy efficiency. The study found that PJS significantly influences thermal comfort in heating situations, while in cooling situations, it mostly affects energy use efficiency. The economic comfort coefficient was developed to identify the best PJSs for cooling and heating intervals under various ventilation strategies, examining indoor thermal comfort and energy consumption efficiency. Compared to the MV, ZV, and DV, the SV performed better in reducing the spread of infection and illness.

Furthermore, because the coronavirus spreads by contact with extremely tiny droplets or spray residues that stay in the air for several minutes or hours, this is what is called the transmission of infection through the air. A high-efficiency particulate air filter (HEPA) was used to purify the air from the virus. Filters that adhere to the HEPA standard have to perform at a specified degree of effectiveness. According to common standards, a HEPA air filter must remove at least 99.95% or 99.97% of particles having a diameter of 0.3 μm from the air, with filtering efficiency rising for particles with dimensions both less than and larger than 0.3 μm [18], as shown in Fig. 1. Pollen, filth, dust, moisture, bacteria (0.2–2.0 μm), viruses (0.02–0.3 μm), and submicron liquid aerosol (0.02–0.5 μm) are all captured by HEPA filters [19]. Particles of every size are removed by all filters. Every filtering mechanism is active at all times (i.e., straining, impaction (impingement), interception, diffusion, and electric charge). In all size ranges, filters' efficacy varies greatly. Even the tiniest of particles can be partially removed by a window screen. The biggest particles will all be eliminated by a HEPA filter. The WHO further advises that the noise level in an occupied classroom should not exceed 40 dBA and that in an empty classroom, the noise level should not exceed 35 dBA [20]. All HEPA air purifiers produce white noise, which does not negatively affect humans but rather helps improve work performance.

Many research studies have examined the spread of infection within the classroom, but they fell short in terms of energy savings and the impact of the different places where the source of infection was within the classroom. Furthermore, there is no research that specifically identifies the best conditioning regimen for efficient infection management, according
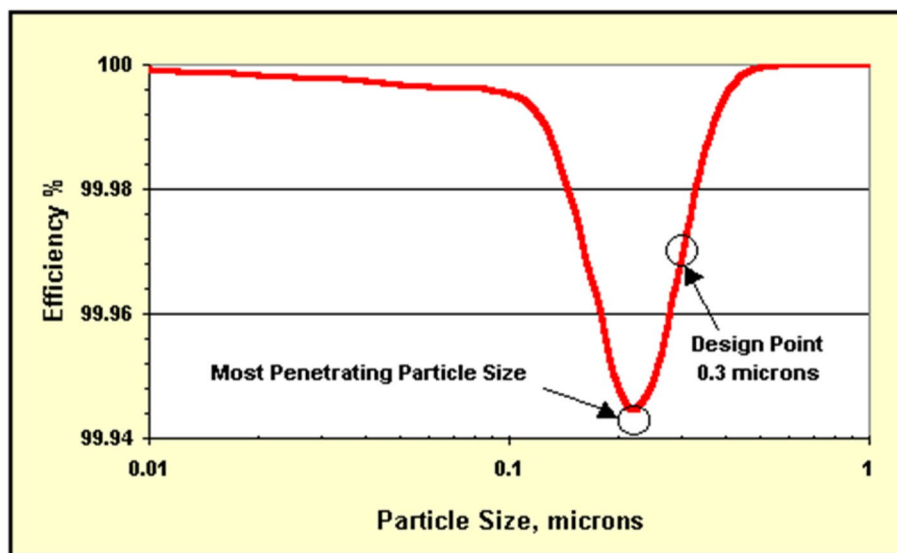
ElShimi *et al. Journal of Engineering and Applied Science*   (2024) 71:19

Page 5 of 39

Fig. 1 HEPA filter efficiency by particle size [21]

to references [22, 23]. The idea of the research is to return to the normal situation of class-room capacity in the event of any occurrence by designing a transparent cabin separating the students inside the classroom. No one has ever studied such a cabin with a filter in the classroom to control infection among students. In this study, a novel cabin made of highly transparent acrylic was designed to control the spread of the virus and keep saliva particles resulting from sneezing inside it in the event that there were any infected students. Then the saliva particles are withdrawn through the filter fan installed at the top of the cabin, which works by filtering the air and allowing it to return to the classroom after being cleaned so that the virus does not reach another student. In the case of student movement, students must wear masks while entering or leaving the classroom, and the movement of entry and exit must be in an organized, non-random manner to limit the spread of infection.

## Methods

Geometry and computational domain

The CFD program has been used to create a CFD model for a real classroom, which has the main dimensions of length, width, and height of 11.76 m (L) $\times$ 5.18 m (W) $\times$ 2.78 m (H) and is set up with desks and seats, as is customary in classrooms, as shown in Fig. 2. The volume was meshed with 4,305,638 cells using a gambit program with tetrahedral elements, as shown in Fig. 3.

Mesh independency check

In order to simultaneously optimize the model accuracy and computational costs, six different mesh sizes (3 851 352, 4 145 578, 4 150 158, 4 305 638, 4 524 467, and 4 728 343) were investigated at the same boundary and inlet conditions. The test revealed a 5% difference in the velocities and a 3% difference in the temperatures of the coarsest and finest meshes. As shown in Fig. 4, the mesh that was ultimately selected contains 4,305,638 tetrahedral cells, which results in a mean outlet temperature difference of 0.081% from the

(a)
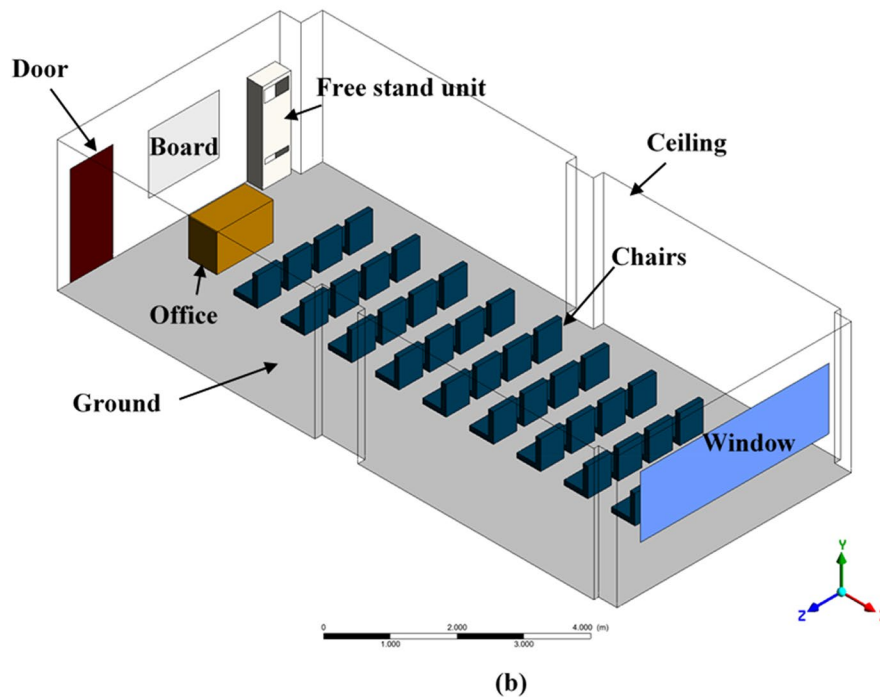
(b)

Fig. 2 Classroom under study **a** real, and **b** CFD model

finest mesh. A variation of less than 3% might be seen when comparing the model's results to those obtained through experimentation. The mouth size is 4 cm × 2 cm, as shown in Fig. 5a, and the mesh of the student and around the mouth is shown in Fig. 5b, c.

Mathematical modelling
Governing equations

Carrier (air) phase　　The CFD program is based on the finite volume approach, which is the foundation of fluid solutions. The domain is discretized into a limited number of

ElShimi *et al. Journal of Engineering and Applied Science*   (2024) 71:19

Page 7 of 39
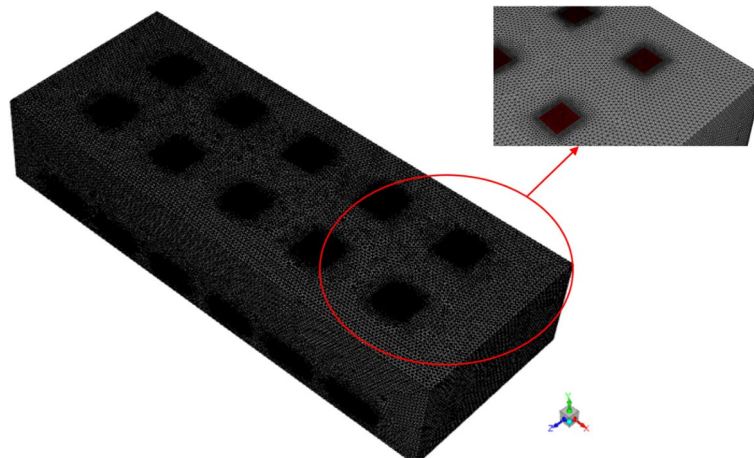
Fig. 3 Mesh of the CFD model
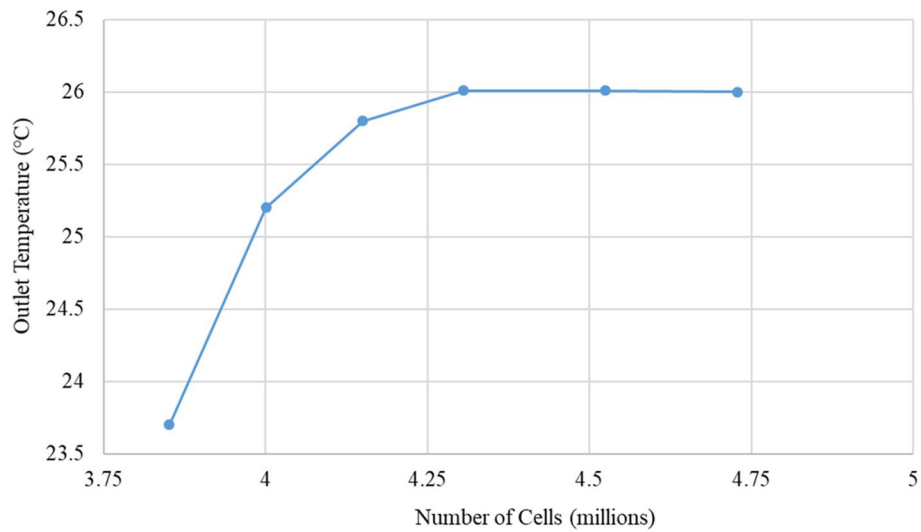
Fig. 4 Outlet temperature at different numbers of cells

control volumes, to which the fundamental conservation equations for mass, momentum, and energy are applied [24].

$$\frac{\partial \rho}{\partial t} + \nabla \bullet \left(\rho \vec{v} \right) = 0 \tag{1}$$

$$\frac{\partial (\rho \vec{v})}{\partial t} + \nabla \bullet \rho \vec{v} \vec{v} = -\nabla P + \nabla \bullet (\overline{\overline{\tau}}) + \rho \vec{g} \tag{2}$$

$$\frac{\partial (\rho E)}{\partial t} + \nabla \bullet (\vec{v}(\rho E + P)) = \nabla \bullet (\rho k_{eff} \nabla T - h + \left(\overline{\overline{\tau}}_{eff} \bullet \vec{v} \right)) \tag{3}$$
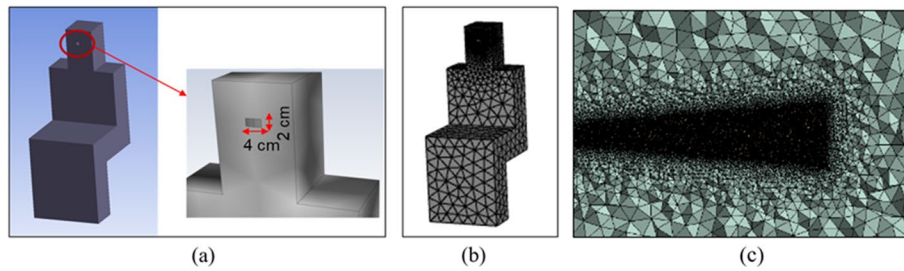
Fig. 5 **a** Dimensions of the mouth, **b** mesh of the student body, **c** mesh around student's mouth

$$E = h - \frac{P}{\rho} + \frac{v^2}{2} \tag{4}$$

where ρ denotes the air density (kg/m3), v denotes velocity (m/s), t denotes the time in seconds, P is the local air pressure (Pa), $\overline{\overline{\tau}}$ represents the stress tensor (Pa), $keff$ represents the effective thermal conductivity (W/m·K), h denotes the enthalpy (J/kg), E denotes the total energy (J), T refers to the air temperature (K), and $\vec{g}$ represents the gravitational acceleration (m/s2). The distribution of species concentrations for H_2O was additionally examined in Eq. 5.

$$\frac{\partial(\rho \vec{v} C_i)}{\partial t} = -\nabla \bullet \vec{Ji} + S_i \tag{5}$$

$$\vec{Ji} = -\rho D_{i.m} \nabla Y_i - D_{T.i} \frac{\nabla T}{T} \tag{6}$$

where Y_i denotes the mass fraction, $\vec{Ji}$ represents the diffusion flux, and $D_{i,m}$ refers to the mass diffusion coefficient of the i_{th} species. $D_{T.i}$ refers to the Soret diffusion coefficient, and S_i refers to the source term.

The RNG-based k-ε turbulence model is derived from the instantaneous Navier–Stokes equations, using a mathematical technique called renormalization group" (RNG) methods. The analytical derivation results in a model with constants different from those in the standard k-ε model, and additional terms and functions in the transport equations for k and ε. The turbulence effect is taken into consideration by using the two-equation k-ε model (i.e., Eqs. 7 and 8), which estimates the turbulence viscosity based on the turbulence's kinetic energy and how it dissipates. The turbulent viscosity in this model is connected to the dissipation rate (ε) and the kinetic energy (k) of the turbulence, as shown by Eq. 9 of the Prandtl-Kolmogorov equation [25]. The RNG k-ε model has a similar form to the standard k-ε model:

$$\frac{\partial(\rho k)}{\partial t} + \frac{\partial(\rho k u_i)}{\partial x_i} = \frac{\partial}{\partial x_j}\left(\alpha_k \mu_{eff} \frac{\partial k}{\partial x_j}\right) + G_k + G_b - \rho\varepsilon - Y_M + S_k \tag{7}$$

$$\frac{\partial(\rho\varepsilon)}{\partial t} + \frac{\partial(\rho\varepsilon u_i)}{\partial x_i} = \frac{\partial}{\partial x_j}(\alpha_\varepsilon \mu_{eff} \frac{\partial\varepsilon}{\partial x_j}) + C_{1\varepsilon}\frac{\varepsilon}{k}(G_k + C_{3\varepsilon}G_b) - C_{2\varepsilon}\rho\frac{\varepsilon^2}{k} - R_\varepsilon + S_\varepsilon \tag{8}$$

$$\mu_t = \rho C_\mu \frac{k^2}{\varepsilon} \tag{9}$$

Where G_k represents the generation of turbulence kinetic energy due to the mean velocity gradients; G_b is the generation of turbulence kinetic energy due to buoyancy; Y_M represents the contribution of the fluctuating dilatation in compressible turbulence to the overall dissipation rate; the quantities α_k and α_ε are the inverse effective Prandtl numbers for k and ε, respectively; S_k and S_ε are user-defined source terms (W/m³·s); μ_t is the turbulent (or eddy) viscosity; C_μ is a constant $= 0.09$; $C_{1\varepsilon}$, and $C_{2\varepsilon}$ are constants.

Discrete (droplet) phase   The main assumptions are [8, 25]:

a) The geometry of the mouth opening was assumed to be a rectangle.
b) The droplets are considered to be spheres of pure water, and the density used for the water droplet was 998 kg/m^3.
c) Sneezing was simplified by assuming that the airflow was only coming from the mouth and not the nose.
d) The injection angle was 0 ° relative to the horizontal direction.
e) The temperature of the respiratory system for sneezing was fixed at 34 ℃.
f) Heat and mass transfer between the air and the droplet are neglected.
g) The particles rebound or suspend on solid surfaces (i.e., walls, floors, ceilings, and human skin).

The momentum equation is solved using the Lagrangian particle tracking technique to determine individual trajectories. By comparing the inertia of the particle to outside forces, the momentum equation can be expressed as:

$$m_p \frac{d\vec{u_p}}{dt} = \vec{F_g} + \vec{F_D} + \vec{F_B} + \vec{F_f}$$
$$= (\rho_d - \rho)V_d g - \frac{3}{4}C_D \frac{\rho}{\rho_d} \frac{m_d}{2R_d}|u - u_d|(u - u_d) \tag{10}$$

where u and u_p are the instantaneous air flow and the sneeze particle velocity, respectively. $\vec{F_g}$ represents the gravitational force, $\vec{F_D}$ represents the Stokes drag force, $\vec{F_B}$ represents the buoyancy force, and $\vec{F_f}$ represents the frictional force. Here, ρ and ρ_d are the airflow and the sneeze particle densities. In Eq. 10, m_d, V_d, and R_d, are the mass, volume, and radius of the sneeze particle, respectively [26]. C_D is the drag coefficient, which can be calculated as a function of the droplet Reynolds number as:

$$C_D = \begin{cases} \frac{24}{R_{ed}} & (R_e < 1)\text{Stokes regime} \\ \frac{20}{R_{ed}^{0.7}} & (1 < R_e < 1000)\text{Transition regime} \\ \frac{10}{\sqrt{R_{ed}}} & (R_e > 1000)\text{Turbulent regime} \end{cases} \tag{11}$$

where $R_{ed} = \frac{\rho|u - u_d|d}{\mu}$, and d is the diameter of the sneeze particles.

The rate of heat energy ($\dot{Q}$) that would need to be removed from a classroom to maintain the temperature in an acceptable range (convective cooling capacity) calculated

from Eq. 12 [27], the mass flow rate, and the change in temperature calculated from Eqs. 13 and 14, respectively:

$$Q = \dot{m} \times C \times \Delta T \tag{12}$$

$$\dot{m} = \rho \times A \times V \tag{13}$$

$$\Delta T = (T_{avg} - T_i) \tag{14}$$

where $\dot{Q}$ is the rate of convective cooling capacity in the classroom, $\dot{m}$ is the mass flow rate of the entrance air, C is the specific heat capacity of the air, and ΔT is the resulting temperature change of the object, T_{avg} is the average classroom temperature, T_i is the inlet air temperature, A is the surface area of the inlets, and V is the velocity of the inlet air.

Error estimation

Two evaluation methods were used to measure the accuracy of the results: method 1 was the root mean squared error (RMSE) of all validation points, and method 2 was the Pearson product-moment correlation coefficient (PPMCC) [12, 28].

$$\text{RMSE} = \sqrt{\frac{\sum_{i=1}^{N} (S_i - E_i)^2}{N}} \tag{15}$$

$$\text{PPMCC} = \frac{\sum_{i=1}^{N} (E_i - \overline{E})(S_i - \overline{s})}{\sqrt{\sum_{i=1}^{N} (E_i - \overline{E})^2 \sum_{i=1}^{N} (S_i - \overline{s})^2}} \tag{16}$$

where E_i refers to the test value, S_i refers to the simulation value, $\overline{E}$ represents the average test value, $\overline{S}$ represents the average simulation value, and N denotes the total number of data points.

Model validation and airflow turbulence modeling

Figure 6 shows the classroom under investigation is a real classroom with main dimensions of 11.76 m (length), 5.18 m (width), and 2.78 m (height). Conditioned air is supplied to the classroom through the free-standing air-conditioning unit of size (1.85 m $\times$ 0.6 m $\times$ 0.35 m), the outlet has main dimensions (0.25 m $\times$ 0.55 m) and the inlet has main dimensions (0.5 m $\times$ 0.55 m). The main heat sources in the classroom are lights and a data projector. The volume was meshed with 4,305,638 cells using a gambit program with tetrahedral elements, as shown in Fig. 3. Three consecutive lines were chosen to make measurements at different positions in the x direction on a plane that cuts the outlet of the air conditioner in the middle. The locations of the three lines are in front of the fan unit (i.e., @ $x=1.5$ m and $z=0.9$ m), in the center (i.e., @ $x=6.5$ m and $z=2.6$ m), and at the back of the classroom (i.e., @ $x=11.5$ m and $z=2.6$ m). The velocity and temperature were measured at 12 points on each line; the distance between them is 20 cm at this level on the specified lines, starting from 10 cm above the ground, as shown in Fig. 6a. The simplified model of classroom configuration shown in Fig. 6b. The boundary conditions of the CFD model validation are shown in Fig. 6b.
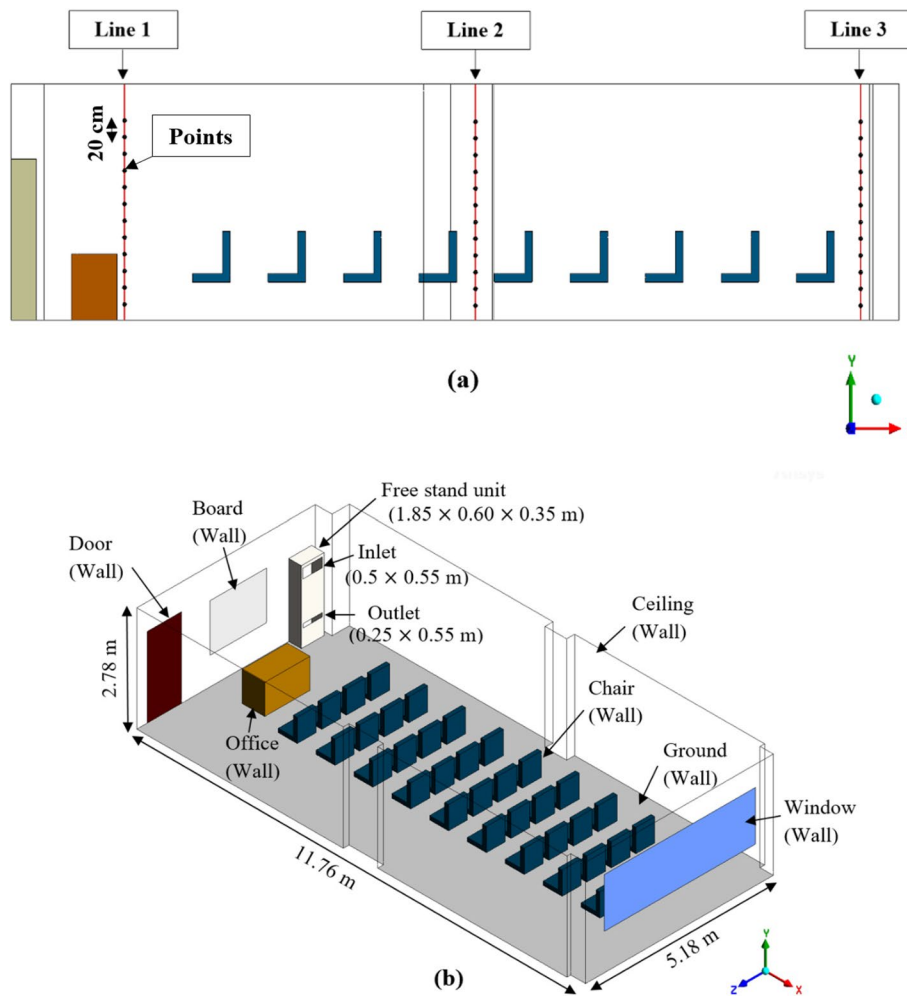
Fig. 6 Validation model, **a** lines and points position of measurements, **b** CFD model boundary condtions

A hot-wire anemometer (AM-4204) was used to measure the mean velocity components and temperatures. A velocity sensor and a temperature sensor are two built-in sensors that are present in the anemometer probe. The accuracy of the hot-wire anemometer is $\pm 5\%$, with a range of velocity between (0.0 m/s and 20.0 m/s. The resolution of the hot-wire anemometer is 0.01 m/s. The resolution of the hot-wire anemometer is (0.1 °C). The anemometer was calibrated before the experiment and checked after the experiment. Figure 7 shows the schematic sketch and the real mechanism to hold the measuring instruments.

Experiments were done with more than one turbulence model to know which was closest to the experiments as well as to determine the best number of meshes in the classroom. Figure 8a, b illustrates that the CFD results for velocity in the x-direction and temperature agree well with the experimental data. Several simulation models were used to find the one with the closest results to the experimental results. Compared with the different turbulence models, Standard k-ε, RNG k-ε, Realizable k-ε, k-ω, and Reynold stress, RNG k-ε was the closest in the results to the experimental measurements and took the least time in the convergence solutions [28–30]. Respiratory fluxes are more accurately predicted by the renormalization group (RNG) k-ε

ElShimi *et al. Journal of Engineering and Applied Science*   (2024) 71:19
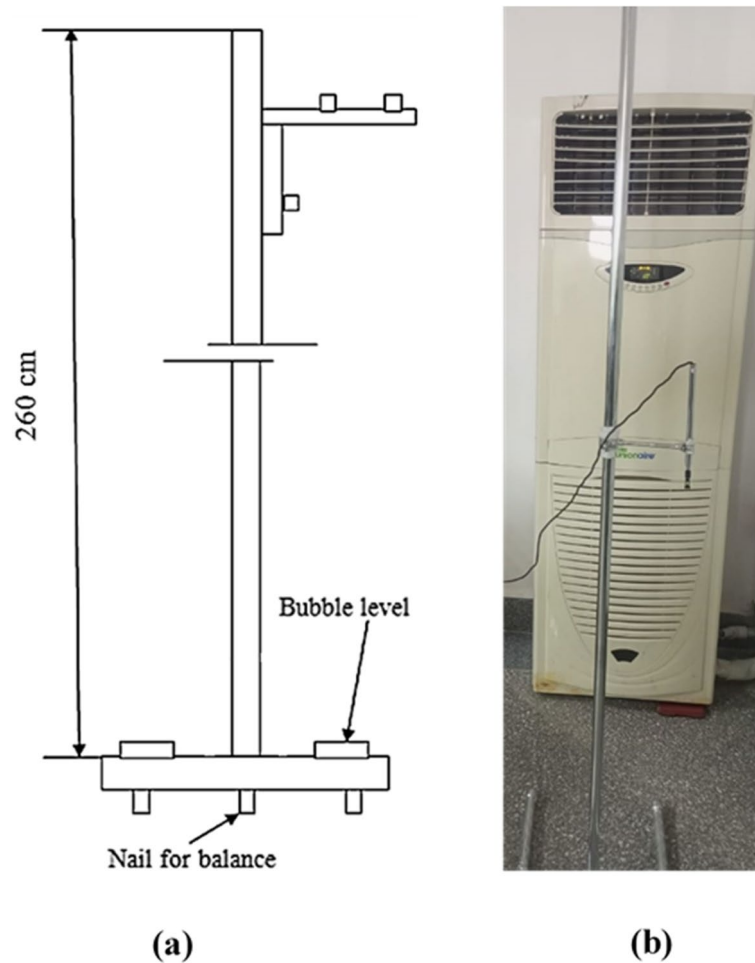
Page 12 of 39

Fig. 7 The mechanism to hold the measuring instrument (i.e., an anemometer) is **a** a schematic sketch mechanism and **b** a real mechanism

model than by the standard and realizable k-ε models [31–33]. The RNG k-ε has generally been extensively used to simulate all types of aerosol movement in indoor settings, including cleanrooms [34, 35].

In comparison to the experimental results, which had RMSE values for velocity and temperature of 0.0681 and 0.2286, respectively, the RNG k-ε model has the lowest RMSE. In order to investigate ways to stop the spread of corona in educational settings, this model was adopted. The PPMCC was thus computed for it, and it was discovered to be equal to 0.9744 for velocity and 0.9984 for temperature.

Lu et al.'s experimental results have been used as the basis for the second validation of the Lagrangian discrete model [36]. The dimensions of the room are 5.0 m × 2.4 m × 3.0 m. With the partition in the middle of the room, the room was divided into two zones equal in dimensions (i.e., zones 1 and 2). The partition has an opening that is a door, the dimensions of which are equal to 0.95 m in height and 0.7 m for width. In addition, in comparison to the room's size, the thickness of the partition is disregarded. A supply and exhaust diffuser is located on the front and back walls; the dimensions are 1.0 m × 0.5 m for the length and height,
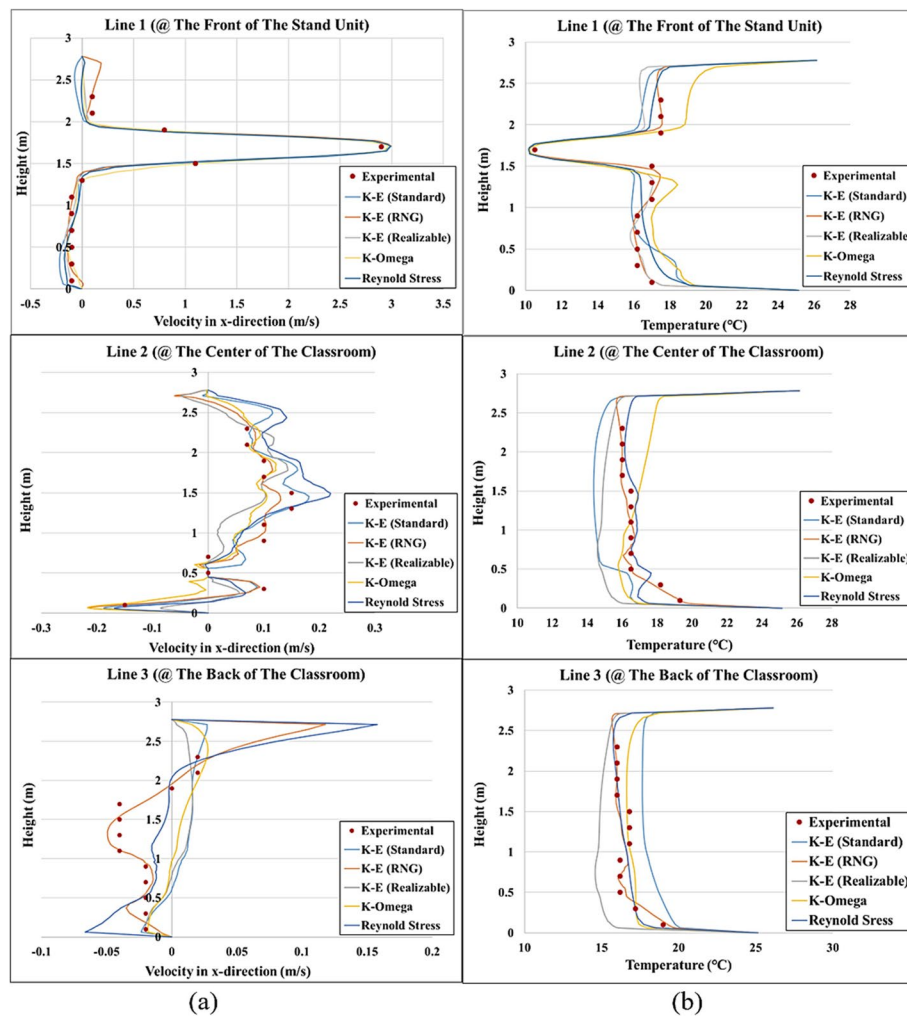
Fig. 8 Comparisons between experimental and CFD simulation along three lines: **a** *x*-velocity component, **b** temperature

respectively, as shown in Fig. 9. In zone 1, the air was provided at an input velocity of 0.09216 m/s, and it was withdrawn from zone 2. The particles range in size from 1, 2, 3, 4, and 5 μm. Each of the particles weighs 147.35 g and has a density of 865 kg/m^3. Figure 10 illustrates the good agreement between the experimental findings of Lu et al. [36] and the current model.

Boundary conditions and numerical methods

The boundary conditions used in developing the model are shown in Fig. 11 and listed in Table 1. Additionally, the boundary conditions of each boundary in the discrete phase model are listed in Table 2. The boundary conditions for the presence of the HEPA filter fan at different flow rates are listed in Table 3. The numerical methods listed in Table 4.
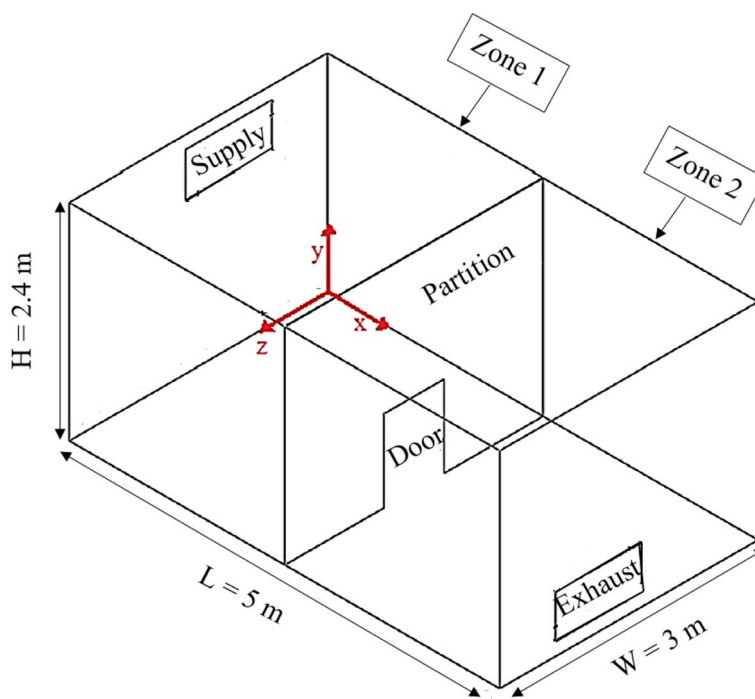
Fig. 9 The Schematic of the three-dimensional two-zone room
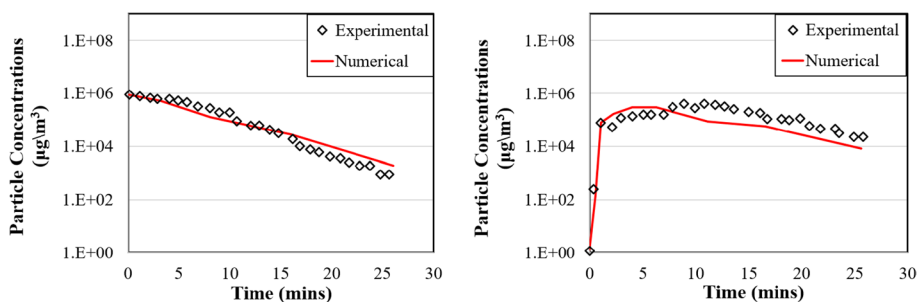
Fig. 10 Comparison of the current model's findings with experimental data [36] **a** for zone 1, **b** for zone 2

Parametric case study

Four different ventilation configurations, along with several influential factors, were studied. Among these is the rate of air change per hour, which varies from 3 to 7 ACH. Also, the height at which the air exits from the ground varies from 0.5 to 2 m. The change in the entry places for fresh air, which is studied for 0.5–2 m heights entering from the side walls of the classroom or the ceiling in the form of one central row or the form of two central rows. Finally, three positions are studied (i.e., at the front, in the middle, and at the back) for the infected student in case of sneezing, as shown in Fig. 12. Thus, there are 12 cases of air distribution shown in Fig. 13, and their specifications are listed in Table 5. In the case of students sitting in the classroom without cabins, the spread of infection was very bad, so cabins were used around each student. The presence of cabins involving each student was investigated to study its effect on preventing the spread of infection in the rest of the classroom and infecting
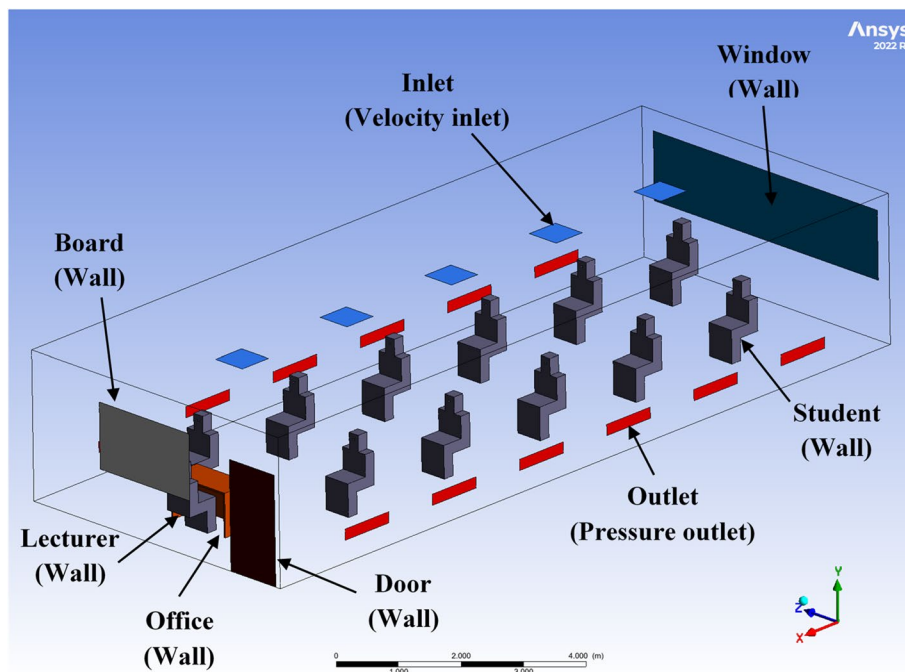
Fig. 11 General layout of the CFD model with boundary conditions

Table 1 Conditions at the generated model's boundaries [25, 26]

Normal breathing

Surface of boundary	Boundary condition	Specifications	Temperature (°C)	Species mass fraction
Inlet	Velocity inlet	From 0.16 to 1.925 m/s	20	$H_2O = 0.008$
Outlet	Pressure-outlet	–	–	$H_2O = 0.008$
Mouth	Mass flow inlet	$m = 0.0002$ kg/s	34	$H_2O = 0.045$ $CO_2 = 0.043$ [37]
Window	Wall	Stationary wall, no-slip	37 (measured)	–
Window wall	Wall	Stationary wall, no-slip	31 (measured)	–
Ceiling	Wall	Stationary wall, no-slip	25 (measured)	–
Sides	Wall	Stationary wall, no-slip	25 (measured)	–
Ground	Wall	Stationary wall, no-slip	24 (measured)	–
Bodies	Wall	Stationary wall; no-slip	Heat Flux = 23.1 W/m^2	–
Office	Wall	Stationary wall, no-slip	Heat Flux = 0 W/m^2	–
Board	Wall	Stationary wall, no-slip	Heat Flux = 0 W/m^2	–
Door	Wall	Stationary wall, no-slip	Heat Flux = 0 W/m^2	–
Sneezing				
Droplet	Mass flow inlet	6.7 mg [38]	34	$\rho = 998$ kg/m^3 $V = 30$ m/s $t = 0.5$ s

Table 2 Boundary conditions in discrete phase model [32, 33, 39]

Boundary name	Boundary condition
Filter inlet, mouth of student, air inlet, air outlet,	Escape
Filter outlet	Reflect
Cabins, board, student body, ceiling, door, ground, lights, office, side walls, window	Trap

Table 3 Boundary conditions of the HEPA filter fan at different flow rates [40, 41]

Velocity (m/s)	Air flow rate (m^3/min)	Pressure drop (Pa)	Number of units
0.45	1.91	− 225	28
0.67	2.84	− 200	28
0.88	3.73	− 185	28
1	4.24	− 195	28
1.33	5.64	− 175	28
1.42	6.02	− 160	28

Table 4 Numerical methods of the developed model [42]

Numerical solution algorithm in steady and unsteady states to solve the Navier–Stokes eq	SIMPLE
Pressure spatial discretization	PRESTO
Momentum spatial discretization	Second order upwind
Energy spatial discretization	Second order upwind
Turbulent kinetic energy spatial discretization	Second order upwind
Turbulent dissipation rate spatial discretization	Second order upwind

others (Fig. 14a), in the case of reducing the number of students in the classroom. The cabin dimensions are 1 m × 0.7 m × 1.5 m with a thickness of 0.01 m (Fig. 14b). In the case of a normal number of students in the classroom, the cabin dimensions are 1 m × 0.7 m × 2 m with a thickness of 0.01 m (Fig. 15). Different dimensions of the cabin were studied, and these mentioned dimensions are the appropriate dimensions for the classroom space and the size of the students, as well as the size of the fan. Where more than one diameter of the fan was studied, it was found that the diameter of 30 cm was the best and most appropriate in limiting the spread of the infection and not leaving saliva particles during sneezing outside the cabin. The findings are shown for both steady-state (normal breathing) and unstable (sneezing).

Cases description

IAQ and energy saving (no infection)

In this part of the study, 12 CFD case simulations involving various HVAC systems were investigated to determine the best design among them in terms of energy savings and indoor air quality (IAQ). Comparing ventilation performance across 12 possible classroom HVAC system configurations and assessing their compliance with the IAQ needs for classroom standards and ASHREA standard values for acceptable CO_2 levels under
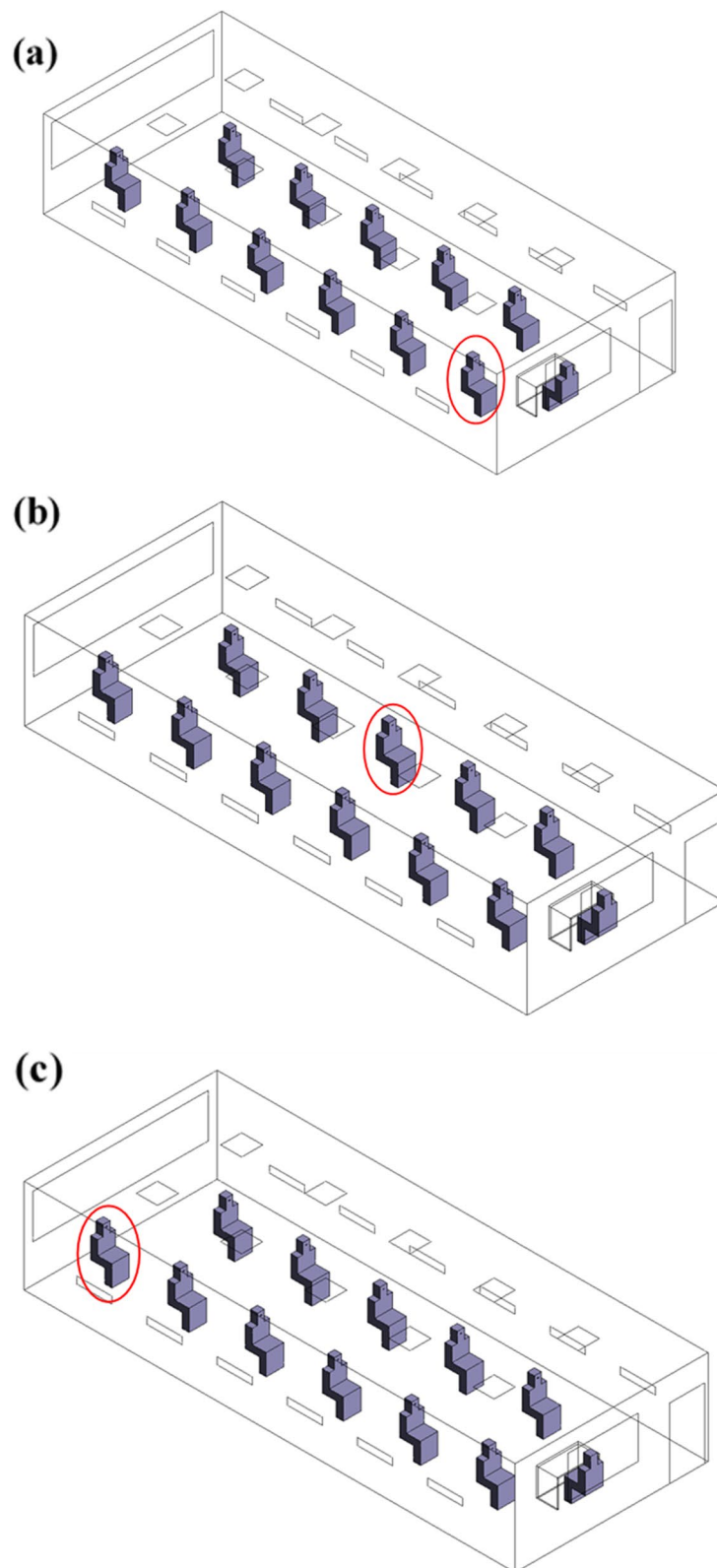
Fig. 12 The position of the infected students, **a** front, **b** middle, **c** back

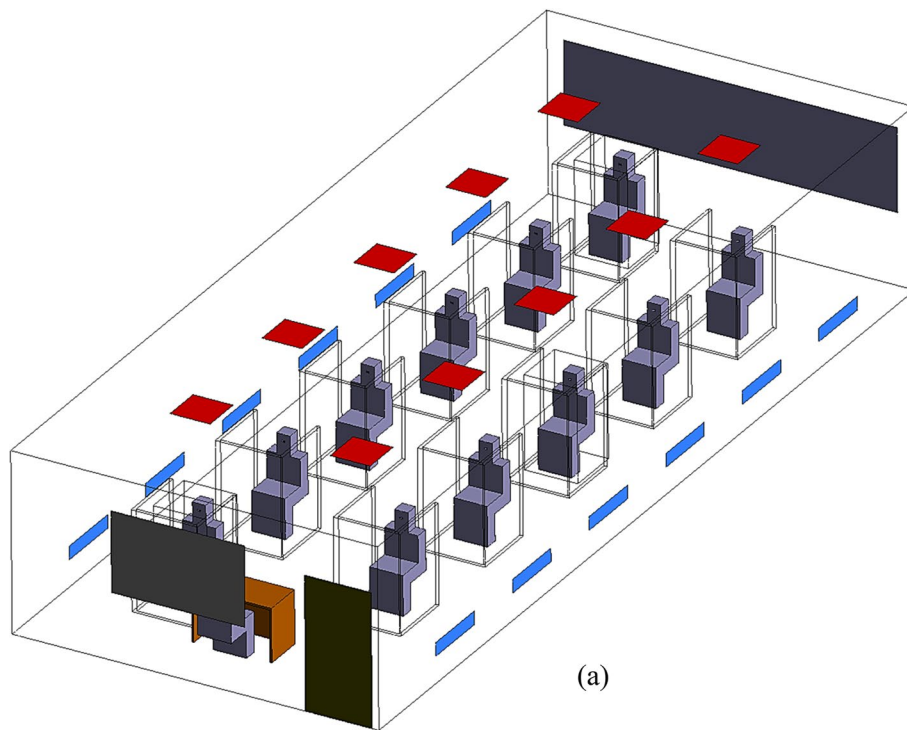| Case No.	Configuration	Case No.	Configuration
1		2	
3		4	
5		6	
7		8	
9		10	
11		12	
	• Blue: inlet grile & Red; outlet grile		

Fig. 13 Configuration of 12 cases

Table 5 Specifications of cases

| Case	Number of supply grilles	Dimensions of supply grilles (m)	Location of supply grilles	Number of exhaust grilles	Dimensions of exhaust grilles (m)	Location of exhaust grilles
1	5	0.6 × 0.6	Located at the centerline of the ceiling (one row)	12	1 × 0.2	Located at low-level, 0.5 m from the floor (two side walls)
2	5	0.6 × 0.6		12	1 × 0.2	Located at low-level, 1 m from the floor (two side walls)
3	5	0.6 × 0.6		12	1 × 0.2	Located at low-level, 2 m from the floor (two side walls)
4	10	0.6 × 0.6	Located at the centerline of the ceiling (two row)	12	1 × 0.2	Located at low-level, 0.5 m from the floor (two side walls)
5	10	0.6 × 0.6		12	1 × 0.2	Located at low-level, 1 m from the floor (two side walls)
6	10	0.6 × 0.6		12	1 × 0.2	Located at low-level, 2 m from the floor (two side walls)
7	6	0.1 × 1	Located at a high-level, 2.5 m from the floor	6	1 × 0.2	Located at low-level, 0.5 m from the floor (one side walls)
8	6	0.1 × 1		6	1 × 0.2	Located at low-level, 1 m from the floor (one side walls)
9	6	0.1 × 1		6	1 × 0.2	Located at low-level, 2 m from the floor (one side walls)
10	12	0.2 × 1	Located at a high-level, 0.5 m from the floor	10	0.6 × 0.6	Located at the ceiling of the classroom (two side walls)
11	12	0.2 × 1	Located at a high-level, 1 m from the floor	10	0.6 × 0.6	
12	12	0.2 × 1	Located at a high-level, 2 m from the floor	10	0.6 × 0.6	

normal breathing (e.g., CO_2 levels not greater than 1000 ppm [18]) were done using numerical data. The rate of change of air was studied from 3 to 8 ACH.

Infection (normal breathing)

As the lowest value advised by ASHRAE in the case of researching ventilation in classrooms, the best-case scenario for regular breathing was created in this section of the study, and the sitting posture of an infected student at ACH equal to 4 was

(a)
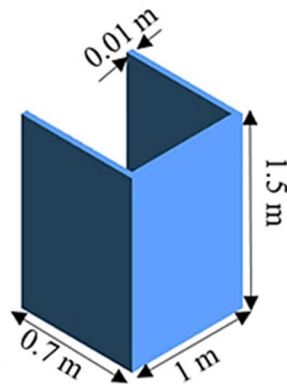
(b)

Fig. 14 In the case of a reduction of the student number in the classroom, **a** layout of the classroom with cabins, **b** configuration of cabin model

examined. Certain assumptions were made about the student to simulate the transmission of the coronavirus. These assumptions included an activity level of 1 met unit, which corresponds to a resting state, a CO_2 generation rate of 0.23 L per minute, a breathing rate of 8 L per minute, and CO_2 as an indicator of airborne contaminants [43]. The gases exhaled by the student were measured at a temperature of 37 and a velocity magnitude of 0.17 m/s, and it was presumed that they were made
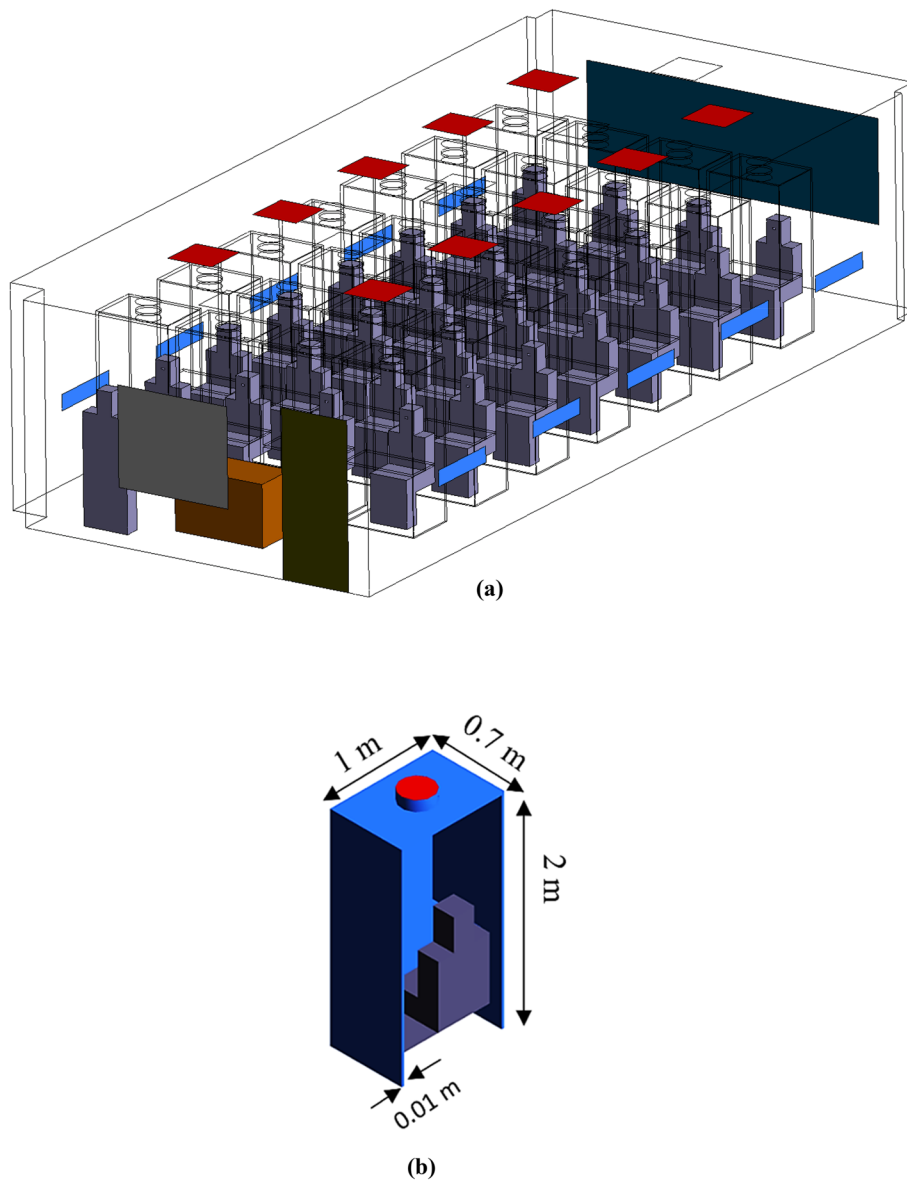
Fig. 15 In the case of a normal number of the student in the classroom **a** layout of the classroom with cabins and filter, **b** configuration of cabin model

up of air, CO_2, and water. CO_2 and H_2O, with mass percentages of 0.043 and 0.045, respectively, made up the expelled gases [44].

Infection (sneezing)

In this part of the study, sneezing will be studied because it is the worst at spreading. There are three cases: the *first* is the presence of a transparent cabinet in which the student sits, which is open from the top, in the case of reducing the number of students in the classroom. In the *second case*, the transparent cabins are closed from the top in the event of a return to the normal number of students in the classroom.
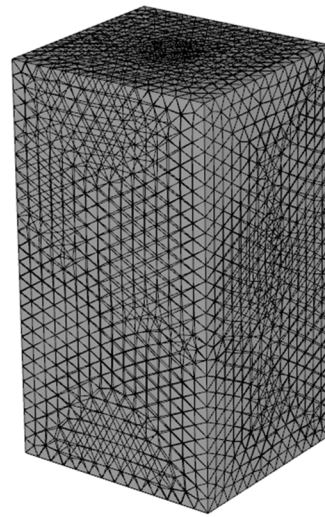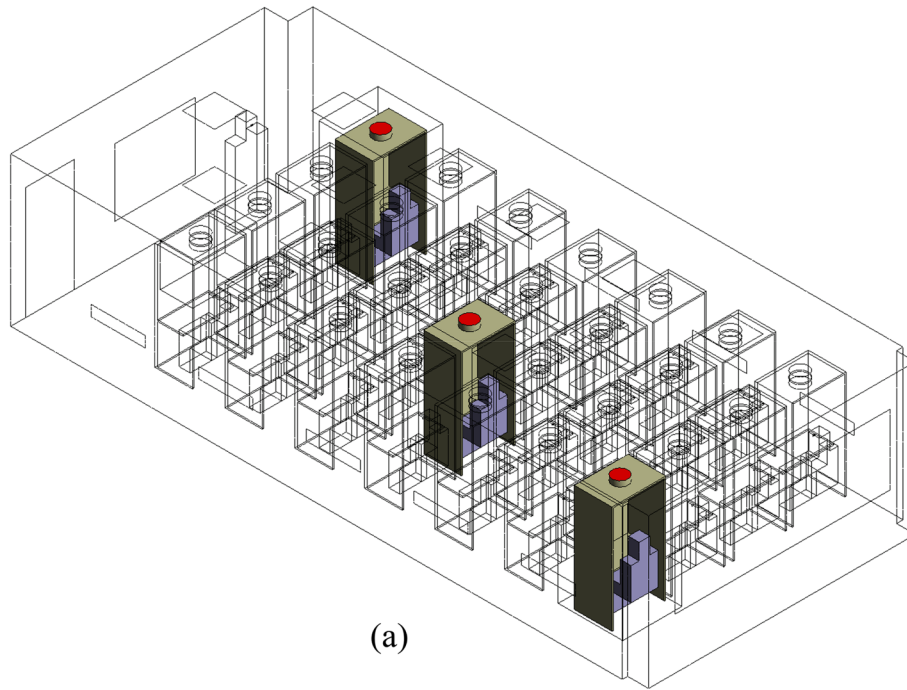
Fig. 16 Different positions of the infected student in the classroom during sneezing for the second and third cases, **a** CFD classroom model, **b** fine mesh for cabin

In the *third case*, the cabins have a filter to remove sneezing particles and let filtered air out from the top for the rest of the classroom.

First case   In the first case, the number of students was equal to 1 per class with opposite seating positions instead of 4 students per row in the absence of infected students. Because the simulation found that the end of the classroom is the worst infection position, the results will be shown for the infected student at the back.
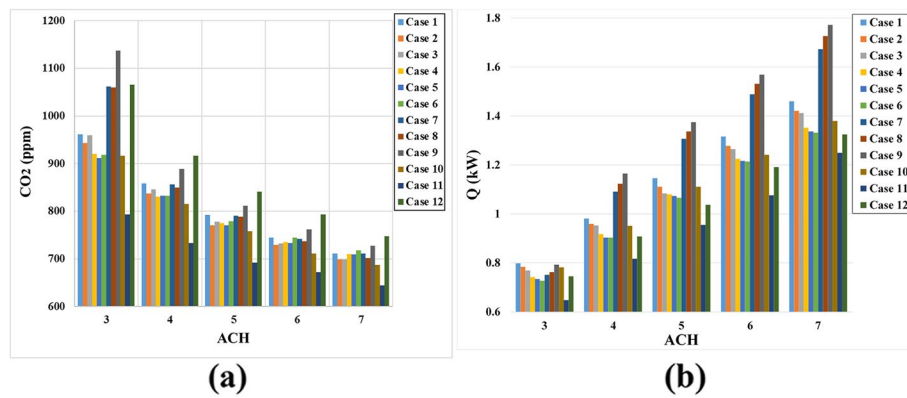
Fig. 17 **a** Average CO_2 concentrations at different ventilation rates at level ($Y = 1.2$ m), **b** cooling load for classroom corresponding to all cases
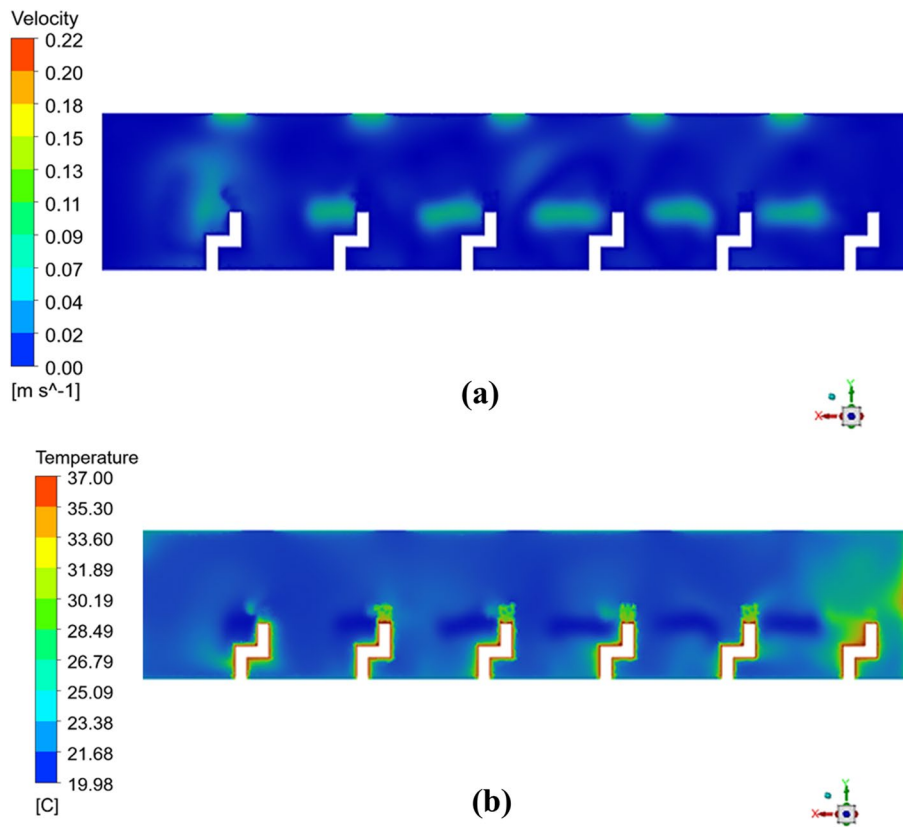
Fig. 18 Air contours around the student body at 4 ACH, **a** velocity, **b** temperature

Second case In the second case, the number of students was equal to 28 in seven rows, with 4 students in each row, with seating positions at equal dimensions in length and width (i.e., in the event of the return of the normal number of students in the classroom) (Fig. 16a). A very fine mesh for the cabin and around the infected student to increase the accuracy of the results (Fig. 16b).
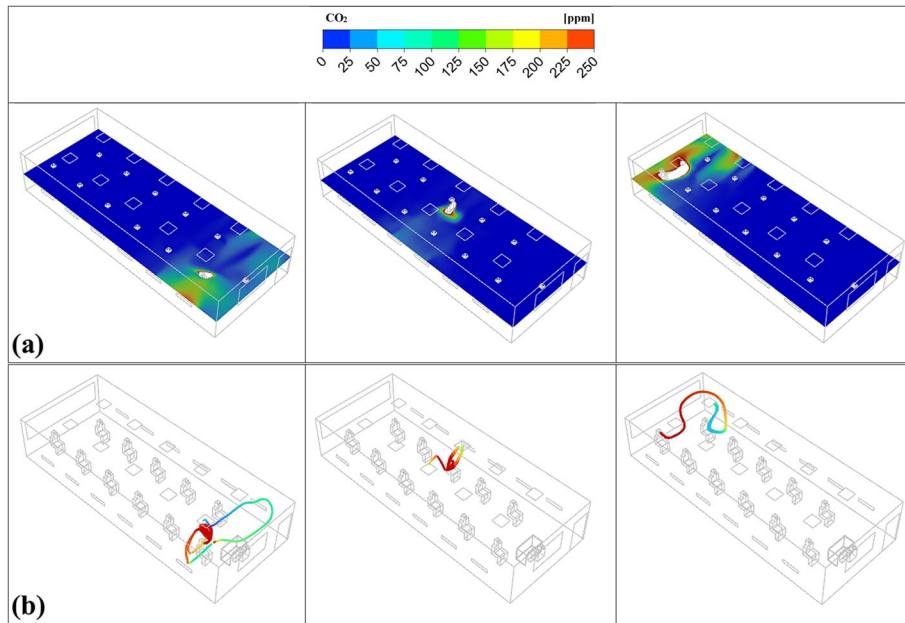
Fig. 19 CFD computed air flow: **a** contaminant contours (ppm) at breathing level ($Y = 1.20$ m); **b** path lines (colored by CO_2 distribution (ppm)) representing contaminant flow
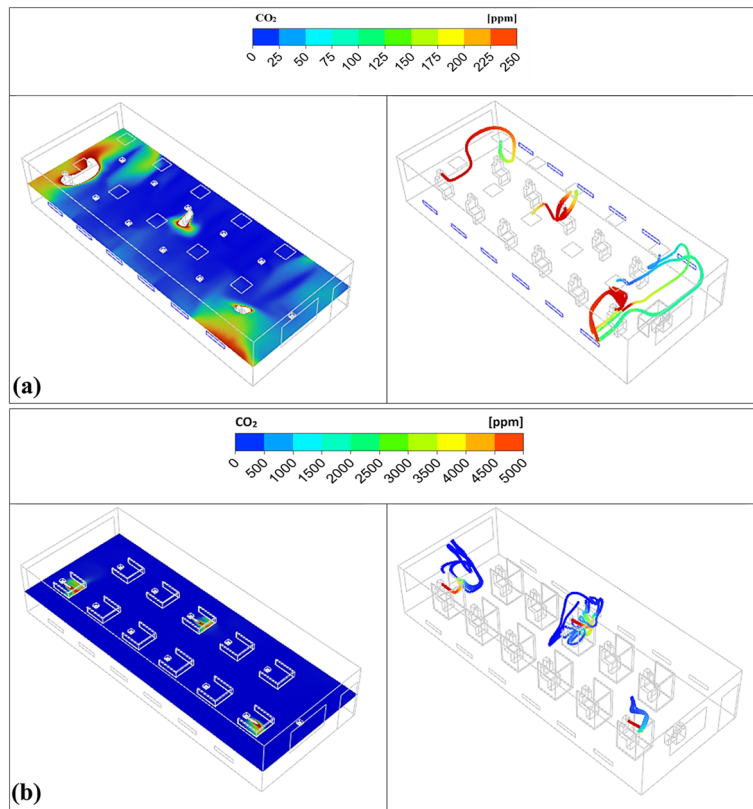

Fig. 20 Infection contours (ppm) at breathing level ($Y = 1.20$ m) and infection path lines (colored by CO_2 distribution (ppm)): **a** without cabins, **b** with cabins
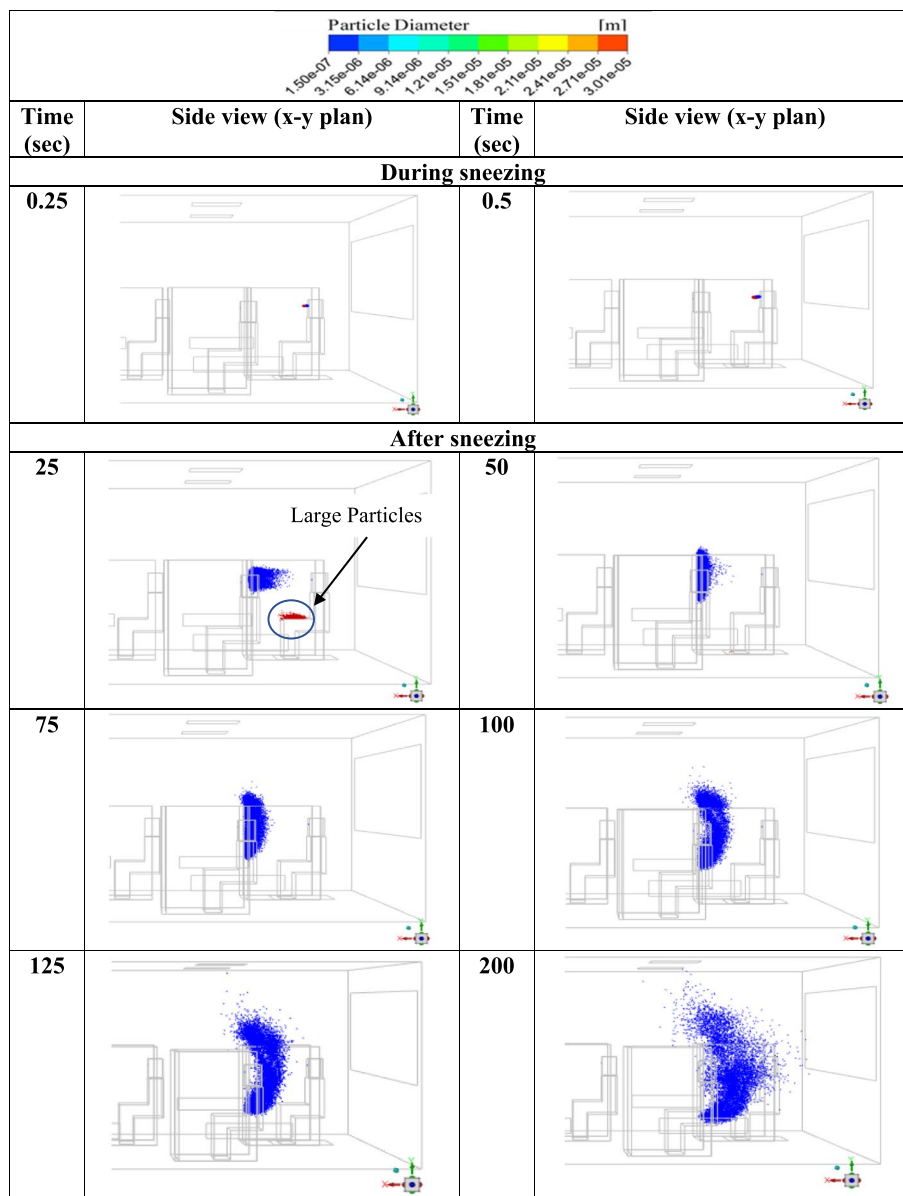
Fig. 21 Particle dispersion at different times for cases with cabins opened from the top with the infected student at the back

Third case In the third case, the filter was operated to remove sneezing particles and purify the air inside the cabin. A HEPA filter was used for this study, and in an occupied classroom, the maximum noise level was 45 dBA. A measurement used to assess the efficacy of air purifiers and other air cleaning systems is the clean air delivery rate (CADR). Modern air purifiers include built-in fans with silent motors, so there won't be a lot of extra noise in the room. The filter with medium speed is the type compatible with this study, which requires the use of 28 filters in the classroom, and the noise is within the permissible limits, which are to be less than 45 dBA. In order to get the proper flow to quickly manage saliva droplets produced by sneezing and prevent them from spreading beyond the cabin, this study used a fan with various flow rates. The different fan flow
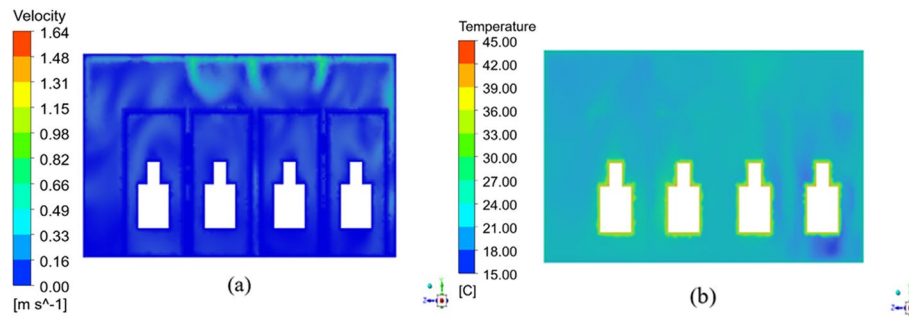
Fig. 22 Air distribution around student bodies at 4 ACH (Y–Z plan) at $x = 5.5$ m, **a** velocity contours, **b** temperature contours

rates on the ceiling of the cabin were studied. For the first range of flow rate, the filter's flow rates for the withdrawal of saliva droplets equal 1.91 to 3.73 m^3/s. Whereas the second range of high filter flow rates ranges from 4.24 to 6.02 m^3/s.

Results and discussion

IAQ and energy saving (no infection)

In normal breathing, it was found that the level of carbon dioxide concentration exceeded the recommended value in the case of 3 ACH only, but starting from 4 ACH, it achieved the acceptable level, and this is what is recommended by ASHREA. From the previous cases, it's clear that increasing the ACH leads to a dilution of the CO_2 level in the classroom, but this leads to an increase in ventilation costs and a lack of energy savings (Fig. 17). The convection cooling capacity in the classroom varies in 12 cases because it depends on the temperature difference between the average temperature of the classroom and the temperature of the incoming air, which varies according to the distribution of air entry and exit points inside the classroom. Therefore, an air change per hour of 4 was chosen in all cases that will be studied later in order to conserve the energy consumed in cooling the classroom. Figure 18 shows the distribution of velocities and temperatures for the case in which the air enters from the side walls at a height of 1 m and exits from two rows in the ceiling for ACH equal 4 around one of the students in the classroom in the $x–y$ plan (i.e., @ $z = 3.8$ m), showing that the temperature is in the recommended range (i.e., the range of temperature from 22 to 26) w.r.t. the ASHREA standard and the velocity is equal to or less than 0.25 m/s at the head/facial region of the occupant to achieve thermal comfort conditions [28]. The best case for ventilation in the classroom is when the air enters from the sidewall and exits from the ceiling because fresh air enters from the bottom and carries viruses to the top, where the air exits and this reduces the spread of the virus among students.

Infection (normal breathing)

Figure 19 shows the distribution of contaminants for case eleven, in which the air enters from the side walls at a height of 1 m and exits from two rows in the ceiling for ACH equal 4 around one of the students in the classroom. Figure 19a shows that at the end of the classroom, near the window and outside wall exposed to the outside atmosphere,
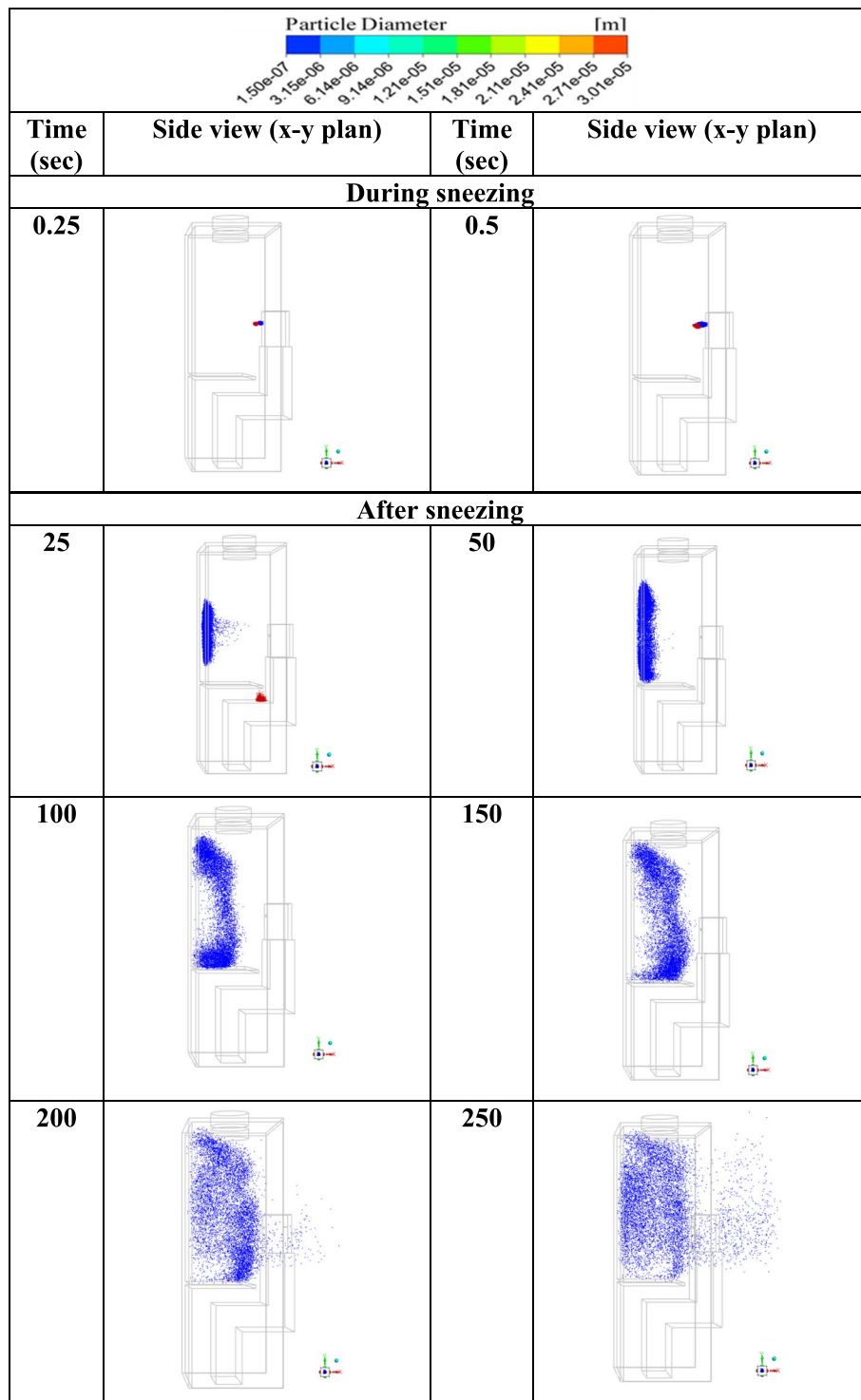
Fig. 23 Particles dispersion at different times for cases with cabin conditions, the filter off, and the infected student at the back

there is a considerable temperature differential that generates an air vortex that serves to both accelerate the transmission of the virus from the nearest infected student and disperse it more widely in the area. Figure 19a, b shows that the greatest spread of infection
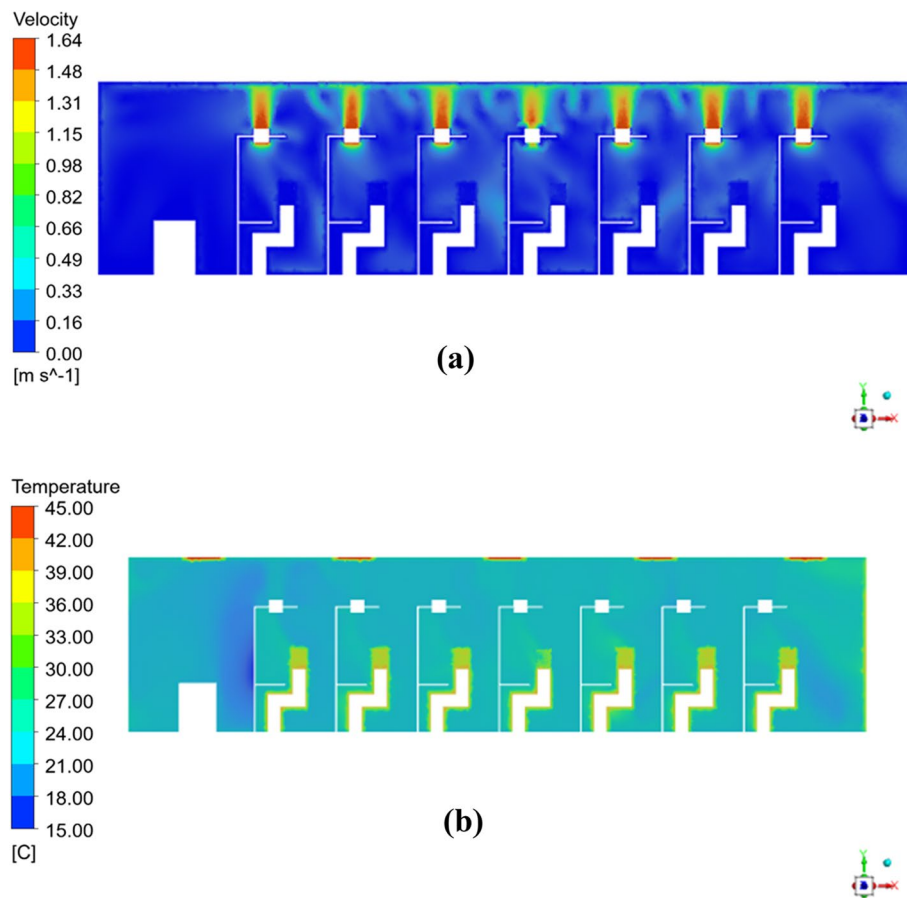
Fig. 24 Air distribution around student bodies at 4 ACH (X–Y plan), **a** velocity contours, **b** temperature contours

Table 6 Results of the presence of the HEPA filter at different velocities

CADR (l/s)	Velocity (m/s)	Noise/unit (dBA) ASHRAE [45]	Time need to remove sneezing particles (s)
38	0.45	30	200
57	0.67	37	100
75	0.88	45	60
85	1	42	35
113	1.33	47	20
121	1.42	50	15

occurs when the infected person is in the front part of the class, followed by the back part, and then in the middle. Figure 20a shows the worst conditions in the case of three infected students by the contours of the contaminant and the path lines. The addition of cabins has helped limit the spread of the virus during normal breathing. This model will work better to lower the chance of infection from the infected student to the rest of the class. The contaminant CO_2 at the level of breathing is confined within the cabins and has not spread to the surrounding area around the infected students. Figure 20b

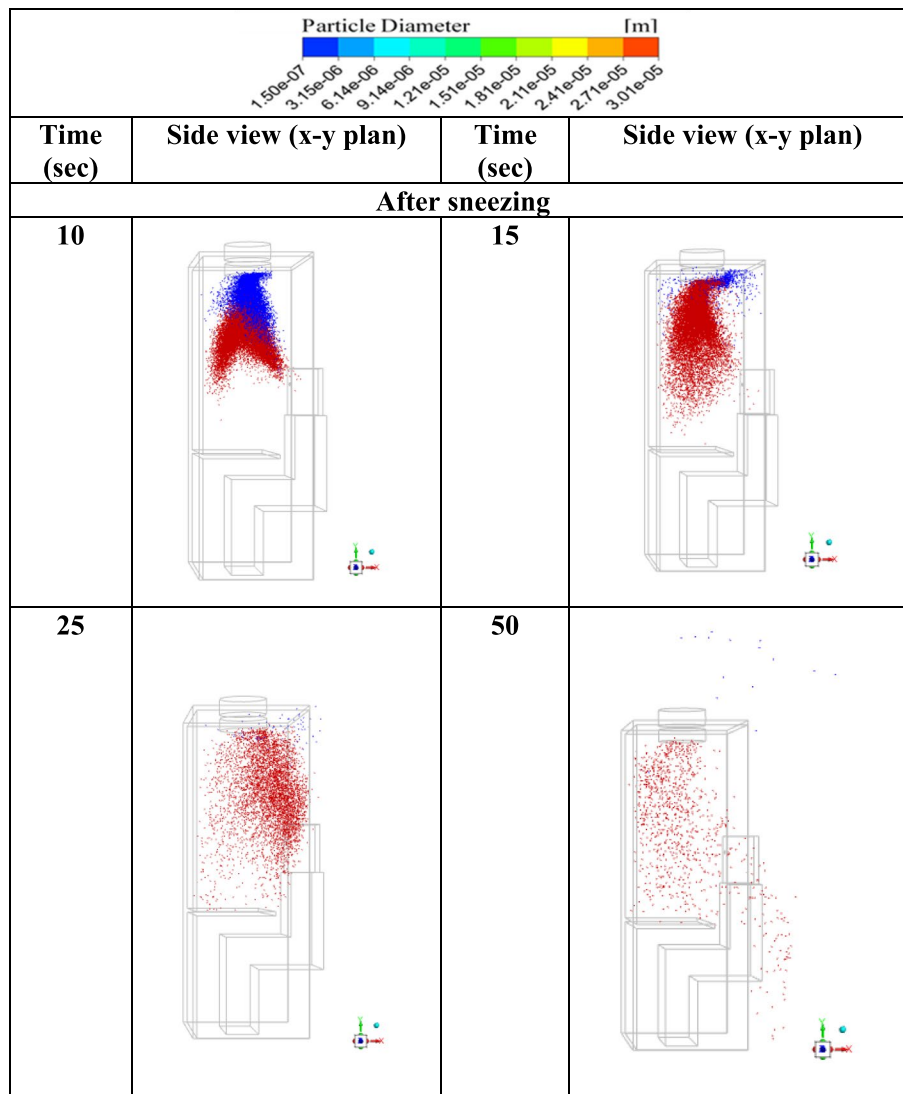| Time (sec)	Side view (x-y plan)	Time (sec)	Side view (x-y plan)
Particle Diameter [m] (1.50e-07, 3.15e-06, 6.14e-06, 9.14e-06, 1.21e-05, 1.51e-05, 1.81e-05, 2.11e-05, 2.41e-05, 2.71e-05, 3.01e-05)		
After sneezing		
10		15	
25		50	

Fig. 25 Particles dispersion for different times for case with a filter fan speed equal 0.45 m/s with the infected student at the back

shows the beginning of the infection path lines exiting from the infected students and that they are directed upwards with the air to the air exit holes directly, without spreading in the classroom. Saliva droplets can travel about 2 m before they touch the ground in the classroom.

Infection (sneezing)

During sneezing, the distances between the particles are very small. After the end of the sneeze (i.e., after 0.5 s), the particles begin to spread in the small area after the sneeze, according to Fig. 21. After each sneeze, more than 6.7 mg of saliva is released at rates as high as 30 m/s.
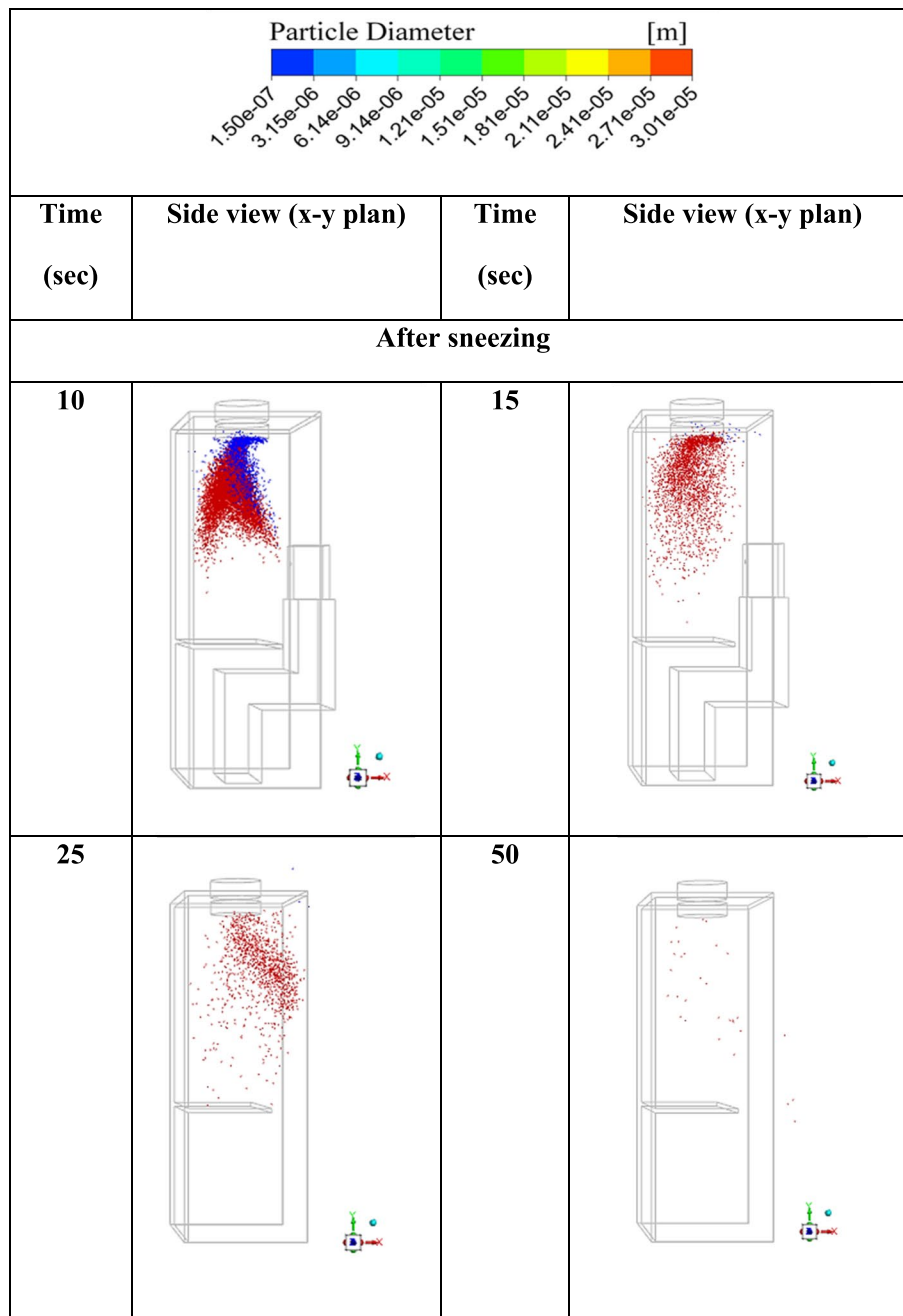
Fig. 26 Particles dispersion for different times for case with a filter fan speed equal 0.67 m/s with the infected student at the back

First case

The simulation of the distribution of sneeze droplets over all students during sneezing at 0.25 and 0.50 s and after sneezing at 25 to 250 s by the CFD program for the positions of the infected student at the back is shown in Fig. 21. After the end of the sneeze, the particles begin to spread in a small area until 25 s after the sneeze. After 25 s of sneezing, it is evident that the large-diameter sneeze particles descend to the desk due to gravity. All of the sneezing particles are contained behind the
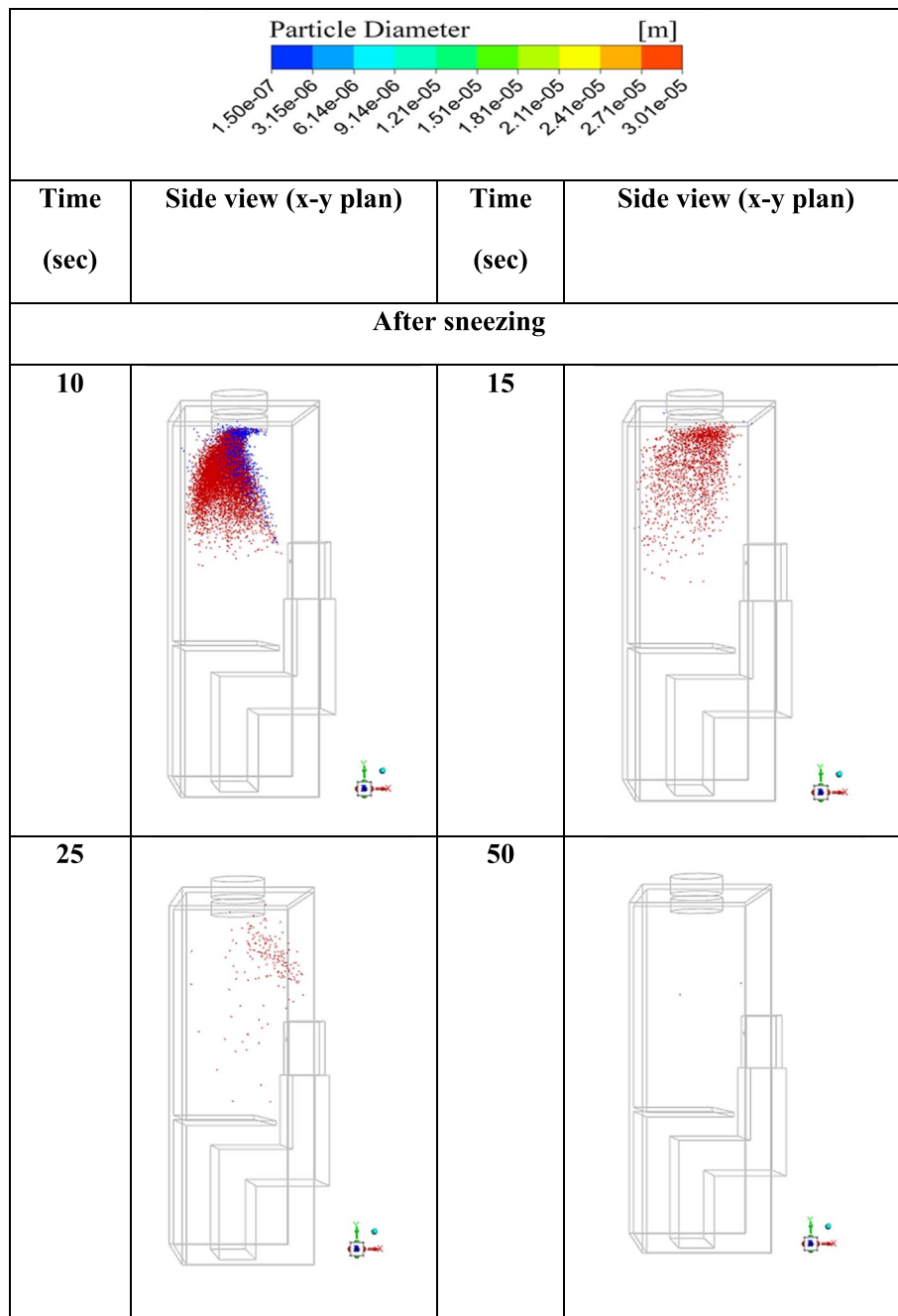
Fig. 27 Particles dispersion for different times for case with a filter fan speed equal to 0.88 m/s with the infected student at the back

transparent cabins 50 s after the sneeze, and none of them escape to harm the other children in the classroom. At 75 s after sneezing, the particles begin to exit from the borders of the cabins and spread in the air surrounding the infected student in the classroom. The particles begin to spread in the air around the infected student in the classroom 75 s after the student sneezes and rises to the top with the direction of the air movement to the exit openings. It takes the microscopic particles
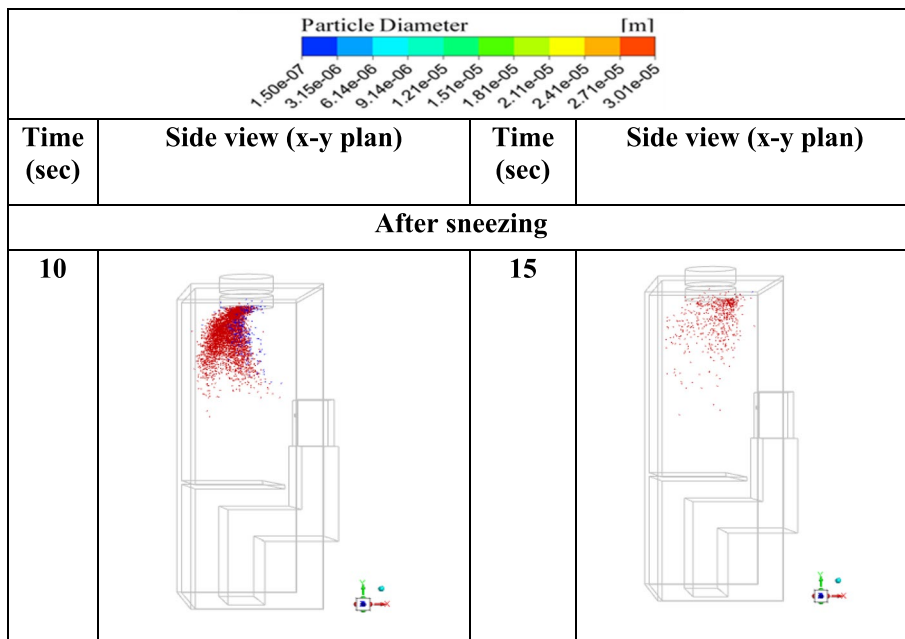
ElShimi *et al. Journal of Engineering and Applied Science*   (2024) 71:19

Page 32 of 39

Fig. 28 Particles dispersion for different times for case with a filter fan speed equal to 1.0 m/s with the infected student at the back
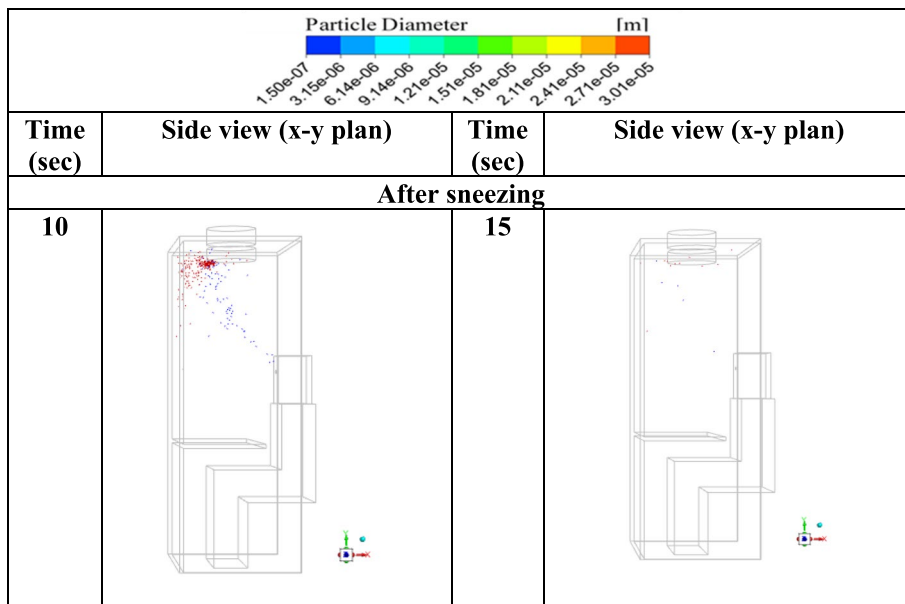

Fig. 29 Particles dispersion for different times for case with a filter fan speed equal to 1.33 m/s with the infected student at the back

125 s after a sneeze to reach the ceiling and start to leave from the top, where the air exit holes are, while still traveling at the same speed as the air in the classroom. All particle sizes, ranging in size from 0.15 to 0.3 μm, are present during and immediately after sneezing. However, over time, the large diameters fall and adhere to nearby objects because there is not enough air to carry them, while the small diameters continue to move with the air and leave the exit openings after a period of up
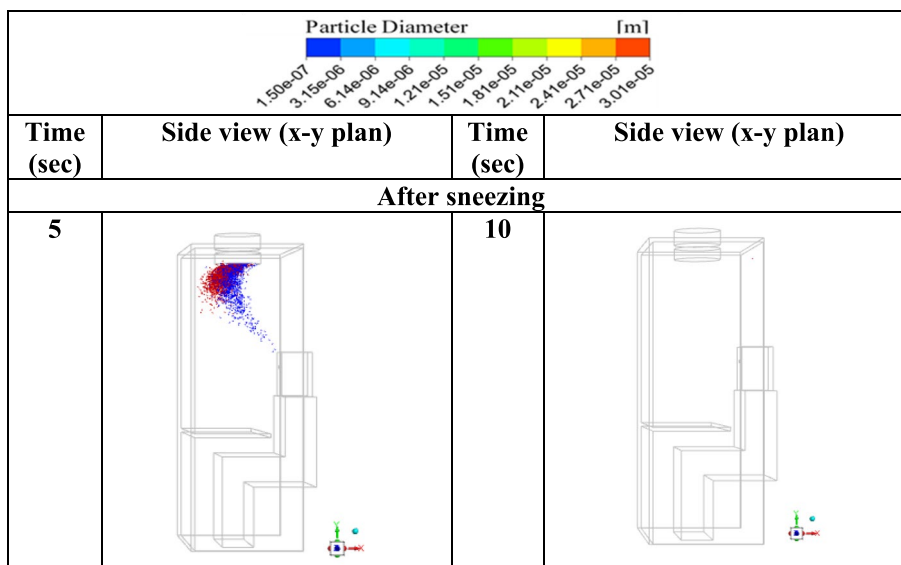
Fig. 30 Particles dispersion for different times for case with a filter fan speed equal 1.42 m/s with the infected student at the back

to 750 s. The particles that are left have just one diameter, based on the aforementioned. The smallest and easiest to transport by air, it has a diameter of 0.15 µm and is the most hazardous since it has been present in the classroom for a long time. This diameter is critical because it can migrate to other parts of the classroom as it evaporates and gets smaller over time.

Second case

The velocity and temperature distribution at the plane intersecting the student bodies for a normal number of students showed that the velocity and temperature around each student did not exceed 0.25 m/s and 26 °C, respectively, which corresponds to the values recommended by ASHREA to achieve thermal comfort for humans [26] (Fig. 22). Figure 23 shows how the CFD software (ANSYS Fluent) modeled the dispersion of sneeze droplets across the classroom at 0.25 and 0.50 s and from 25 to 250 s using various locations of the infected student in the front, in the middle, and at the back, respectively. Particles begin to circulate in the air surrounding the infected student in the classroom 200 s after the infected student sneezes and escapes from the edges of the cabin, and part of these particles begins to move to the rest of the classroom, and another part ascends with the air to the air outlet. In this case, the spread of sneezing particles occurs in the classroom, but at a greater rate than in the previous case, as the cabin is closed from the top in the second case. In the second case, the spread occurred at a lower level within the classroom than it did in the previous case (Fig. 23).
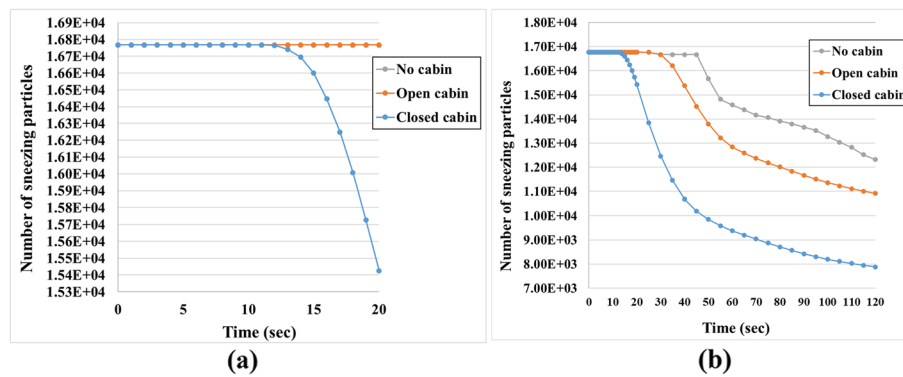
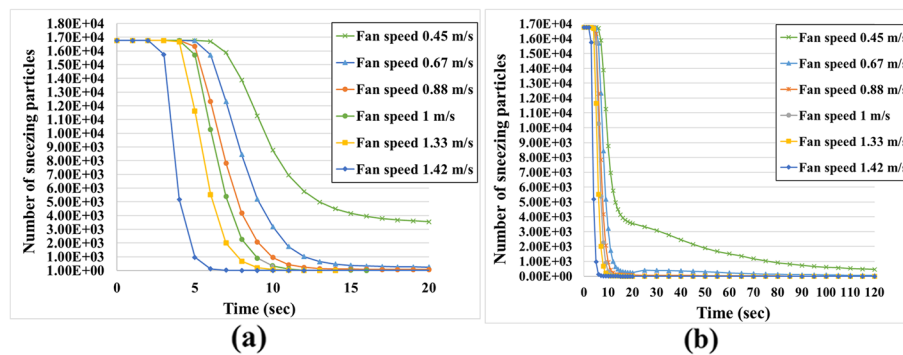**Fig. 31** The number of sneezing particles inside the classroom with time **a** 0.5–20.0 s, **b** 0.5–120.0 s

Fig. 32 The number of sneezing particles inside the classroom at different fan speed with time **a** 0.5–20.0 s, **b** 0.5–120.0 s

Third case

The velocity and temperature contours were shown in Fig. 24 when the filter was working. It was found that the different fan flow rates purify the air inside the cabin from virus-carrying saliva particles, but it takes different time periods according to the fan withdrawal flow rates. The higher the withdrawal flow rate, the shorter the time period for viruses to be present inside the cabin around the infected student, but the increase in flow rates leads to an increase in the noise level, which is within the permissible limits, as listed in Table 6. At the low fan retraction speeds above the infected student inside the cabin, some saliva droplets from sneezing were coming out of the cabin, as shown in Figs. 25 and 26. The presence of the filter worked to fully control the spread of the virus and not leave it outside the cabins for a very short period of up to 70 s after sneezing, after which the virus particles disappeared completely. Therefore, it is the best way to control the spread of the virus in the classroom, and that is also true for the normal number of students. The filter pulls out the light particles first (i.e., 1.5 μ m), then the heavy ones (i.e., 3.01 μ m), until all the particles are withdrawn from inside the cabin (Fig. 26). When flow rates were increased from the permissible value for the filter to reach 4.24, 5.64, and 6.02 m^3/s (i.e., fan speeds are 1, 1.33, and 1.42 m/s), it was found that the duration of filter withdrawal for viruses decreased to 35, 20, and 15 s, respectively. Figures 27, 28, 29 and 30 illustrate particle dispersion for a case with a filter fan speed equal to 0.88, 1, 1.33, and 1.42 m/s with the infected student (i.e., flow rates of 3.73, 4.42, 5.64, and 6.02 m^3/s), respectively, at the back at the same time. The value of

the CADR for these speeds is equal to 85, 113, and 121 L/s, which is matched by noise values equal to 42, 47, and 50 dBA, respectively.

The saliva after sneezing happened at the filter entrance after 10 s, and because the fan speed was insufficient to remove the big particles, they dropped to the bottom due to gravity, as illustrated in Fig. 25 Within 15 to 25 s, the particles started to spread within the cab, and after 50 s, I got out. Therefore, in this situation, the fan speed is insufficient.

According to Fig. 26, after 10 s, particles start to gather at the filter intake; at 15 s, large-diameter particles start to spread further inside the cabin as a result of their weight and the fan's inability to draw them; and at 25 s, they start to spread even more. Then, due to their weight, the particles started to depart the chamber after 50 s. But when we compare the speed of 0.67 m/s to the speed of 0.45 m/s, we discover that while the speed of 0.67 m/s is the best, it is also insufficient to remove all the particles.

Figure 27 illustrates the flow of sneeze particles at a speed of 0.88 m/s as particle aggregation happens 10 s after sneezing, and by 15 s, the image demonstrates that all small-sized particles have been dragged out. It becomes apparent that there are heavy particles, although they are few in quantity, at a speed of 25 m/s. The particles don't seem to be leaving the chamber at all, though. A control was also implemented within the cabin when it was discovered that there were hardly any spit flecks left at 50 s. It is obvious that at this pace, salivary particles were tightly under control and were not exiting the cabin. In contrast to the earlier speeds (0.45), this one is the best. In comparison to the earlier speeds (0.45 m/s and 0.67 m/s), this is the best speed.

Figures 28, 29 and 30 indicate that as fan speed is increased, sneeze particles are sucked in more quickly and become trapped inside the cabin. The likelihood of virus transmission reduces as the fan's intake speed increases because sneeze particles are removed more rapidly and in less time, using more energy for the fan in the process.

The number of sneezing particles produced by three infected students in the classroom was studied in different cases. Figure 31 represents the number of sneezing particles during 120.0 s inside the classroom for several cases: there is no cabin, there is a cabin with an open top, and there is a closed cabin. Figure 31a shows the number of sneezing particles after sneezing (i.e., 0.5 s) to 20 s after the end of sneezing. It is clear that up to 20 s after sneezing, the number of particles is the same in the case where there is no cabin around the students as in the case of an open cabin because the study was for the number of particles in the classroom in general, not in a specific place inside. After approximately 30 s, the number of particles begins to decrease more in the case of an open cabin around each student than in the case of no cabin. In the case of a closed cabin around each student, the number of particles is the same as in the absence of a cabin and the presence of an open cabin until 13 s after sneezing, after which the number of particles will be much less. Figure 31b shows that the minimum number of particles is achieved if there is a closed cabin around each student in the classroom. This difference in the number of particles in the three cases results from the increased presence of surfaces to which particles adhere during sneezing, which leads to the spread of the coronavirus throughout the classroom among students. It turns out that the existence of the cabin helps to drive the particles above, where they are then expelled from the air exit holes in the ceiling. The significant difference between

the number of particles in the three cases began 13 s after the end of sneezing, which is the time of the beginning of the spread of particles away from infected students.

After that, the number of particles was studied in a closed cabin around each student, and it was equipped with a filter and a fan to withdraw the air laden with these particles, purify them from the virus, and leave them in the classroom again. The number of particles resulting from sneezing was studied in the case of operating the fan at several different speeds. Figure 32 represents the number of sneezing particles during 120.0 s inside the classroom for cases of the fan working at different speeds. The number of particles is very large after the sneezing time is over (i.e., 0.5 s). In the beginning, the number of particles is constant for all speeds, as shown in Fig. 32a, so as not to start spreading inside the cabin, and once they spread, part of the particles begin to stick to the nearby surfaces of the cabin, and the other part is pulled upward by the filter fan. It has been found that when the fan speed is increased, more saliva particles are drawn through the filter, resulting in a reduction in the number of particles inside the classroom, as shown in Fig. 32b, which helps in controlling the spread of infection outside the classroom. It is clear from Fig. 32b that the faster the fan draws in virus-laden air, the shorter the time for eliminating saliva particles resulting from sneezing.

Conclusions

In this study, the effects of different air conditioning design variables on the classroom were investigated using a CFD program in the case of an affected student. By using numerical analysis, a thorough study of the frequency of saliva droplets caused by sneezing in the classroom was conducted. The control of infection transmission by saliva droplets from sneezing was considered in light of the analytical findings. As well as how to control infection under normal operating conditions in the classroom. Since it has not been studied before, control the spread of infection inside the classroom by using a transparent cabin around each student. However, during the movement of students to sit in the cabins, masks must be used to prevent the spread of infection from the infected student to the rest of the students in the classroom. The following are the conclusions of the current study:

1. Experiments were done with more than one turbulence model to know which was closest to the experiments as well as to determine the best number of meshes in the classroom.
2. The best case of ventilation in the classroom is when the air enters from the sidewall (at a height equal to 1 m from the ground) and exits from the ceiling (i.e., case 11), because fresh air enters from the bottom and carries viruses to the top, where the air exits, and this reduces the spread of the virus among students.
3. It has been shown that the saliva droplets in the air flow are inversely correlated with the air change per hour in the classroom.
4. The air density drops when temperatures are high close to a wall that is exposed to the sun. This causes a high recirculation of saliva droplets in the case of an infected student in this location, which accelerates the spread of infection.
5. Saliva droplets as small as 0.15 μm are affected by gravity in a sneeze because of the tiny size of the droplets. Therefore, the airflow has the most impact on how they move. Furthermore, drops 20 to 30 μm in diameter or greater are severely gravitationally impacted and fall to the ground.

ElShimi *et al. Journal of Engineering and Applied Science*   (2024) 71:19

Page 37 of 39

6. Saliva droplets can travel about 2 m before they touch the ground in the classroom. This is consistent with the study presented by Zhu et al. [38].

7. The presence of cabins with HEPA filters from above had a strong effect on controlling the spread of the virus in the classroom during sneezing.

8. The increase in filter withdrawal speed is inversely proportional to the time taken for virus particles to be withdrawn.

9. The faster the fan pulls in virus-laden air, the fewer sneezing particles there will be inside the classroom.

To control the spread of the coronavirus in the classroom, there must be a cabin. If they are open at the top, they direct particles up and out of the air outlet holes in the ceiling. If it is closed at the top and has a filter to purify the air from viruses, it directs the particles upwards towards the filter so that they then come out pure for the rest of the classroom students. However, cabin surfaces must be sanitized after each class session because some saliva particles stick to them after sneezing.

Abbreviations

ACH	Air Change per Hour
ASHRAE	American Society of Heating, Refrigerating, and Air-Conditioning Engineers
CFD	Computational Fluid Dynamics
CO_2	Carbon dioxide
COVID-19	Coronavirus disease 19
HEPA	High-Efficiency Particulate Air filter
HVAC	Heating Ventilation and Air Conditioning
IAQ	Indoor Air Quality
SIMPLE	Semi-Implicit Method for Pressure Linked Equation

Declarations

Competing interests
The authors declare that they have no competing interests.

References
1. Hiscott J et al (2020) Cytokine and growth factor reviews the global impact of the coronavirus pandemic. Cytokine Growth Factor Rev 53:1–9. https://doi.org/10.1016/j.cytogfr.2020.05.010
2. Kong X et al (2021) Experimental study on the control effect of different ventilation systems on fine particles in a simulated hospital ward. Sustain. Cities Soc. 73:103102. https://doi.org/10.1016/j.scs.2021.103102
3. Kumar S, King MD (2022) Numerical investigation on indoor environment decontamination after sneezing. Environ. Res 213:113665. https://doi.org/10.1016/j.envres.2022.113665

4.   Chillón SA, Fernandez-Gamiz U, Zulueta E, Ugarte-Anero A, Urbina-Garcia O (2023) Numerical modeling of a sneeze, a cough and a continuum speech inside a hospital lift. Heliyon 9(2):1–15. https://doi.org/10.1016/j.heliyon.2023.e13370

5.   T. Dbouk and D. Drikakis, "On airborne virus transmission in elevators and confined spaces," Phys. Fluids, 2021; 33 (1):, https://doi.org/10.1063/5.0038180

6.   Yamakawa M, Kitagawa A, Ogura K, Chung YM, Kim M (2021) Computational investigation of prolonged airborne dispersion of novel coronavirus-laden droplets. J. Aerosol Sci. 155:105769. https://doi.org/10.1016/j.jaerosci.2021.105769

7.   Ascione F, De Masi RF, Mastellone M, Vanoli GP (2021) The design of safe classrooms of educational buildings for facing contagions and transmission of diseases: a novel approach combining audits, calibrated energy models, building performance (BPS) and computational fluid dynamic (CFD) simulations. Energy Build 230:110533. https://doi.org/10.1016/j.enbuild.2020.110533

8.   Arpino F, Cortellessa G, D'Alicandro A, Grossi G, Massarotti N, Mauro A (2023) CFD analysis of air supply rate influence on the aerosol dispersion in a university lecture room. Build Environ 235:110257. https://doi.org/10.1016/j.buildenv.2023.110257

9.   A. Adwibowo, "Computational fluid dynamic (CFD), air flow- droplet dispersion, and indoor CO2 analysis for healthy public space configuration to comply with COVID 19 protocol," medRxiv and bioRxiv, 2020

10. F. Akagi, I. Haraga, S. I. Inage, and K. Akiyoshi, Effect of sneezing on the flow around a face shield, Phys. Fluids, 2020; 32 (12): https://doi.org/10.1063/5.0031150

11. Gök K, Selçuk AB, Gök A (2021) Computer-aided simulation using finite element analysis of protect against to coronavirus (COVID-19) of custom-made new mask design. Trans Indian Inst Met 74(5):1029–1033. https://doi.org/10.1007/s12666-021-02227-4

12. Bahramian A, Mohammadi M, Ahmadi G (2023) Effect of indoor temperature on the velocity fields and airborne transmission of sneeze droplets: an experimental study and transient CFD modelling. Sci Total Environ 858:159444. https://doi.org/10.1016/j.scitotenv.2022.159444. (October 2022)

13. Ying F, O'Clery N (2021) Modelling COVID-19 transmission in supermarkets using an agent-based model. PLoS One 16(4):1–13. https://doi.org/10.1371/journal.pone.0249821

14. Vernez D, Schwarz S, Sauvain JJ, Petignat C, Suarez G (2021) Probable aerosol transmission of SARS-CoV-2 in a poorly ventilated courtroom. Indoor Air 31(6):1776–1785. https://doi.org/10.1111/ina.12866

15. Srivastava S, Zhao X, Manay A, Chen Q (2021) Effective ventilation and air disinfection system for reducing coronavirus disease 2019 (COVID-19) infection risk in office buildings. Sustain Cities Soc 75:103408. https://doi.org/10.1016/j.scs.2021.103408

16. C. Ren, H. Zhu, and S. Cao, Ventilation strategies for mitigation of infection disease transmission in an indoor environment : a case study in office. 2022; 1: https://doi.org/10.3390/buildings12020180

17. Li H, Fu Z, Xi C, Li N, Li W, Kong X (2022) Study on the impact of parallel jet spacing on the performance of multi-jet stratum ventilation. Appl Energy. 306:118135. https://doi.org/10.1016/j.apenergy.2021.118135

18. Godoy C, Thomas D (2020) Influence of relative humidity on HEPA filters during and after loading with soot particles. Aerosol Sci Technol 54(7):790–801. https://doi.org/10.1080/02786826.2020.1726278

19. Payet S, Boulaud D, Madelaine G, Renoux A (1992) Penetration and pressure drop of a HEPA filter during loading with submicron liquid particles. J Aerosol Sci 23(7):723–735. https://doi.org/10.1016/0021-8502(92)90039-X

20. Canada A (2019) SAC–OAC-2019-Classroom-Acoustics_EN

21. W. J. Kowalski, W. P. Bahnfleth, and T. S. Whittam, Filtration of airborne microorganisms: Modeling and prediction, ASHRAE Trans. 1999; 105

22. Ding E, Zhang D, Bluyssen PM (2022) Ventilation regimes of school classrooms against airborne transmission of infectious respiratory droplets: a review. Build. Environ. 207:108484. https://doi.org/10.1016/j.buildenv.2021.108484

23. Chan WR et al (2020) Ventilation rates in California classrooms: why many recent HVAC retrofits are not delivering sufficient ventilation. Build. Environ. 167:106426. https://doi.org/10.1016/j.buildenv.2019.106426. (August 2019)

24. John D (2003) Anderson, Modern Compressible Flow, 3rd edn

25. Menni Y et al (2022) Effects of two-equation turbulence models on the convective instability in finned channel heat exchangers. Case Stud. Therm. Eng. 31:101824. https://doi.org/10.1016/j.csite.2022.101824. (May 2021)

26. ANSYS FLUENT, ANSYS Fluent Theory Guide, ANSYS Inc., USA, 2013; 15317: 1–759, [Online]. Available: http://www.pmt.usp.br/ACADEMIC/martoran/NotasModelosGrad/ANSYS Fluent Theory Guide 15.pdf

27. Wang H, Zhu J, Dai Y, Hu H (2023) A simplified cooling load calculation method based on equivalent heat transfer coefficient for large space buildings with a stratified air-conditioning system, no

28. M K Owen, D S Ensor. "A i r b o r n e particle sizes a n d s o u r c e s f o u n d i n i n d o o r air m k, 1992; 26(12): 2149–2162

29. Rohdin P, Moshfegh B (2007) Numerical predictions of indoor climate in large industrial premises. a comparison between different k-ε models supported by field measurements. Build Environ 42(11):3872–3882. https://doi.org/10.1016/j.buildenv.2006.11.005

30. D'Alicandro A, Mauro A (2023) Experimental and numerical analysis of CO 2 transport inside a university classroom: effects of turbulent models. J Build Perform Simul 16:1–26. https://doi.org/10.1080/19401493.2022.2163423

31. D'Alicandro A, Mauro A (2021) Effects of operating room layout and ventilation system on ultrafine particle transport and deposition. Atmos Environ 270:118901. https://doi.org/10.1016/j.atmosenv.2021.118901

32. P. Taylor, Numerical Heat Transfer , Part B : Fundamentals : An International Journal of Computation and Methodology a comparison of different solution methodologies for melting and solidification problems in enclosures, no. September 2012, 37–41, 2007

33. Bahramian A, Mohammadi M, Ahmadi G (2023) Effect of indoor temperature on the velocity fields and airborne transmission of sneeze droplets: an experimental study and transient CFD modeling. Sci. Total Environ. 858:159444. https://doi.org/10.1016/j.scitotenv.2022.159444. (July 2022)

34. D'Alicandro AC, Mauro A (2023) Air change per hour and inlet area: Effects on ultrafine particle concentration and thermal comfort in an operating room. J. Aerosol Sci. 171:106183. https://doi.org/10.1016/j.jaerosci.2023.106183

35. Liu Z, Zhang M, Cao G, Tang S, Liu H, Wang L (2021) Influence of air supply velocity and room temperature conditions on bioaerosols distribution in a class l operating room. Build. Environ. 204:108116. https://doi.org/10.1016/j.buildenv.2021.108116

36. Lu W, Howarth AT, Adam N, Riffati SB (1996) Modelling and measurement of airflow and aerosol particle distribution in a ventilated two-zone chamber. Build Environ 31(5):417–423. https://doi.org/10.1016/0360-1323(96)00019-4

37. A. E. A. Eldegwy, E. E. Khalil, S. M. Morcos, and E. M. Elbialy, NUMERICAL INVESTIGATIONS OF INDOOR AIR QUALITY IN American Institute of Aeronautics and Astronautics American Institute of Aeronautics and Astronautics, 1–12, 2015

38. Zhu SW, Kato S, Yang JH (2006) Study on transport characteristics of saliva droplets produced by coughing in a calm indoor environment. Build Environ 41(12):1691–1702. https://doi.org/10.1016/j.buildenv.2005.06.024

39. Luo Q et al (2022) Role of pathogen-laden expiratory droplet dispersion and natural ventilation explaining a COVID-19 outbreak in a coach bus. Build. Environ. 220:109160. https://doi.org/10.1016/j.buildenv.2022.109160

40. "Data sheet Fan Systems." [Online]. Available: https://kongskilde-industries.com/industrial/wp-content/uploads/sites/3/123001909-EXP-GB-Fan-Systems-DATA-0518.pdf

41. We A (1996) Industrial fans. Met Finish 94(7):61. https://doi.org/10.1016/s0026-0576(96)98350-6

42. Oh W, Ooka R, Kikumoto H, Han M (2022) Numerical modeling of sneeze airflow and its validation with an experimental dataset. Indoor Air 32(11):1–15. https://doi.org/10.1111/ina.13171

43. McLaughlin JB (1989) Aerosol particle deposition in numerically simulated channel flow. Phys Fluids A 1(7):1211–1224. https://doi.org/10.1063/1.857344

44. M. Loomans and T. Lemaire, Particle concentration calculations using CFD, Proc. Roomvent, 2002; 393–396

45. S. T. Taylor et al., Ventilation for acceptable indoor air quality. 1999; 1999: 404–636

Publisher's Note

Springer Nature remains neutral with regard to jurisdictional claims in published maps and institutional affiliations.